Earth and Planetary Science Letters 304 (2011) 468–482

Contents lists available at ScienceDirect

Earth and Planetary Science Letters

journal homepage: www.elsevier.com/locate/epsl

Resetting, errorchrons and the meaning of canonical CAI initial $^{26}Al/^{27}Al$ values

Justin I. Simon [a,*], Edward D. Young [b]

[a] Astromaterials Research Office KR111, NASA Johnson Space Center 2101 NASA Parkway, Houston, TX 77058, United States
[b] Department of Earth and Space Sciences & Institute for Geophysics and Planetary Physics, University of California at Los Angeles, 595 Charles E. Young Drive East, 2676 Geology Building, Los Angeles, CA 90095, United States

ARTICLE INFO

Article history:
Received 29 January 2010
Received in revised form 12 February 2011
Accepted 14 February 2011

Editor: T.M. Harrison

Keywords:
solar nebula
chronology
26Al
open system resetting
isochrons
CAIs

ABSTRACT

The difference between the precise MC-ICPMS analyses of bulk calcium–aluminum-rich inclusion (CAI) fragments (e.g., Jacobsen et al., 2008) and supra-canonical values obtained by micro-analytical techniques, e.g., laser ablation MC-ICPMS (Young et al., 2005) and SIMS (Taylor et al., 2005), at face value seems to be problematic and therefore leads many to dismiss claims of the solar system $(^{26}Al/^{27}Al)_0$ greater than ~5×10^{-5} as spurious. Here we use mass balance calculations to quantify the importance of open system isotopic exchange during CAI evolution and show that *in situ* supra-canonical, *in-situ* canonical, and bulk canonical measurements can all exist for an individual CAI. The calculations describe mechanisms of isotopic exchange that may have occurred early (100's ka) and late (~1.5 Ma) in the solar nebula and much later (>10's Ma) on parent body planetesimals. A range of possible modal mineralogies is modeled in order to populate the compositional space defined by *in situ* and bulk CAI measurements. In support of these simulated data we describe *in situ* measurements of $^{27}Al/^{24}Mg$, $^{25}Mg/^{24}Mg$, and $^{26}Mg/^{24}Mg$ obtained by LA-MC-ICPMS comprising core-to-rim traverses across three CV3 CAIs. The CAIs exhibit distinctive Mg isotopic zoning profiles and varying abundances of daughter products of the short-lived nuclide ^{26}Al that are consistent with varying amounts of open system isotope exchange.

Published by Elsevier B.V.

1. Introduction

Excesses in ^{26}Mg ($^{26}Mg^*$) that correlate with $^{27}Al/^{24}Mg$ in calcium–aluminum-rich inclusions (CAIs) are produced by the decay of ^{26}Al during CAI formation. The correlation among minerals with varying Al/Mg can define an initial $^{26}Al/^{27}Al$ ratio for the object of interest (i.e., an internal isochron). Likewise the correlation among CAIs or fragments of CAIs with varying Al/Mg can be used to define an initial $^{26}Al/^{27}Al$ ratio for the population of objects (i.e., a "whole rock" isochron). The presence of ^{26}Al (mean life = 1.05 Ma) provides a high-resolution relative chronometer for the first ~4 Ma of the history of the solar system if it can be assumed that the initial concentration of ^{26}Al (or $^{26}Al/^{27}Al$) was uniform. It is commonly assumed that the canonical initial $^{26}Al/^{27}Al$ for the solar system as a whole, $(^{26}Al/^{27}Al)_0$, corresponds to an absolute age of ~4568 Ma (e.g., Amelin et al., 2002; Bouvier and Wadhwa, 2010; Bouvier et al., 2007; Jacobsen et al., 2008) and represents the initial abundance of ^{26}Al present during condensation of CAIs. Based on many studies of CAIs this solar-system wide canonical value is 4.5 to 5×10^{-5} (e.g., MacPherson et al., 1995), although more recently some high precision bulk analyses support a slightly higher value of ~5.2×10^{-5} (Jacobsen et al., 2008) (cf. Galy et al., 2000; Thrane et al., 2006; Tonui et al., 2008) that is consistent with early studies (Lee et al., 1976). Claims of supra-canonical $(^{26}Al/^{27}Al)_0$ values based on micro-analytical techniques (i.e., laser ablation MC-ICPMS, Young et al., 2005) instead suggest that at least some CAIs condensed prior to canonical time and that objects yielding canonical ^{26}Al have experienced resetting due to high-temperature events incurred by CAIs during their residence time in the protoplanetary disk.

The idea of using an isochron age based on fragments representing the whole rock to see back through younger resetting events comes from the field of metamorphic petrology and geochemistry (Compston and Jeffery, 1959) and the concept that the "whole-rock" or bulk material of a certain size remains an effectively closed system during later thermal events. This approach is applicable for dating parent body processes. It is unclear, however, whether it is appropriate for a population of CAIs, because these objects almost certainly behaved as open systems (e.g., Aléon et al., 2007; Fagan et al., 2007).

The purpose of the present paper is three-fold: (1) to quantitatively demonstrate how some *in situ* measurements can be supra-canonical within a bulk CAI that is canonical, (2) to test whether nebular reprocessing could be the event(s) recorded by the canonical $^{26}Al/^{27}Al$ values in CAIs, and (3) to provide examples of resetting in the nebula by examining the Al–Mg isotope systematics of well-characterized CAIs. An improved understanding of these key issues will inform our interpretations of the meaning of $^{26}Al/^{27}Al$ values recorded by Mg isotope ratios in CAIs.

* Corresponding author.
E-mail address: Justin.I.Simon@NASA.gov (J.I. Simon).

0012-821X/$ – see front matter. Published by Elsevier B.V.
doi:10.1016/j.epsl.2011.02.023

Despite their primitive nature most CAIs are not pristine nebular condensates (e.g., Grossman et al., 2002). The textures, mineralogies, and compositions of CAIs are complex and likely reflect substantial reprocessing. It has been suggested that once condensed, CAIs experienced a range of histories in the solar nebula that may have included melting, crystallization, evaporation, re-condensation, re-melting, and metamorphism (e.g., Hsu et al., 2000; Hutcheon, 1982; Ireland et al., 1992; Ito et al., 2004; Niederer and Papanastassiou, 1984; Podosek et al., 1991; Richter et al., 2002; Ryerson and McKeegan, 1994; Shahar and Young, 2007; Simon et al., 2005; Stolper, 1982; Young et al., 2002). It should be noted that the majority of micro-analytical $(^{26}Al/^{27}Al)_0$ measurements made are found to be canonical, see review by MacPherson et al. (1995), including those by Young et al. (2005). The importance of this observation should be clear: There is no question about the ubiquity and therefore the importance of a canonical $^{26}Al/^{27}Al$ value. The question is rather, what event(s) in the early solar system do canonical initial $^{26}Al/^{27}Al$ values record? Does canonical time represent the time of major Al/Mg fractionation in the solar nebula, the major CAI melting events, or, as explained here, the major cessation of high temperature thermal processing and isotopic resetting in the nebula?

Evidence for excess ^{26}Mg ($^{26}Mg^*$) is inextricably linked to the measurement of stable Mg isotopes. Theoretical and experimental studies provide a basis for our understanding of the stable Mg isotope composition of planetary materials, in particular with respect to isotope effects related to evaporation at low nebular pressures (Davis et al., 1990; Esat et al., 1986; Galy et al., 2000; Grossman et al., 2000; Richter et al., 2002). Compositional variations due to open system isotopic exchange likely occur at higher nebular pressures as well. At higher pressures, CAIs act as a sink, as well as the source, of Mg. An example of this behavior in CAIs is presented by Simon et al. (2006) who suggest that the low $\delta^{25}Mg$ margins defining the outer portion of core-to-rim isotopic zoning profiles of CAIs represent isotopic exchange with a chondritic gas.

An important question is whether a similar process might also affect the $^{26}Mg^*$ chronologies of CAIs. In order to test this possibility we present a model that accounts for mineral specific isotopic exchange with an external reservoir (e.g., nebular gas or chondrite matrix). Given the modal mineralogy of CAIs and their respective Mg diffusivities, mass balance calculations can be used to model bulk CAI measurements. This modeling provides some insight into the significance of results obtained by different analytical methods and therefore can inform our interpretation of the differences found among micro-analytical and bulk Mg isotope measurements.

Evidence that ^{26}Al–$^{26}Mg^*$ chronologies have been affected by open system isotope exchange can be seen by *in situ* ultraviolet (UV) LA-MC-ICPMS measurements of $^{27}Al/^{24}Mg$, $^{25}Mg/^{24}Mg$, and $^{26}Mg/^{24}Mg$ along core-to-rim traverses of igneous CAIs. The LA-MC-ICPMS data described herein suggest a general correlation between $(^{26}Al/^{27}Al)_o$ and core-to-rim Mg isotope fractionation patterns. In the samples studied, supra-canonical $(^{26}Al/^{27}Al)_o$ values (Young et al., 2005) correspond to relatively constant $^{25}Mg/^{24}Mg$ across the CAIs while canonical $(^{26}Al/^{27}Al)_0$ values correspond to systematic edge-ward deceases in $^{25}Mg/^{24}Mg$. The latter pattern is consistent with isotopic exchange with a nebular gas that has an isotopic composition similar to bulk chondrites. These results support the idea that early Al–Mg isotopic resetting resulted in the preponderance of canonical $(^{26}Al/^{27}Al)_0$ values (Young et al., 2005). Modeling of Mg isotope diffusion and comparisons with these data suggest that CAIs pass through regions of relatively high temperature and high Mg partial pressure on $\leq 10^2$ year time scales. Shock fronts in the solar protoplanetary disk could be the source of the brief high-T, high-P events.

2. Sources of disturbed Al–Mg isochrons

At issue is the meaning of internal isochrons and model isochrons obtained from fragments of CAIs. Internal mineral and bulk Al–Mg isochron systems should respond differently in response to thermal events that can mobilize isotopes, just as in other geological isotopic systems (e.g., Rb–Sr, Sm–Nd, U–Pb). In order to obtain meaningful age information by either technique an assessment of the parameters affecting chemical and isotopic closure for the event under investigation is required. If the Al–Mg system remains effectively closed to isotope exchange for bulk CAIs (or substantial fragments of CAIs such as those measured), a population of CAIs can be used to date their initial crystallization and segregation from nebular gas. Concordance of isochrons obtained from bulk samples to those obtained by the internal mineral isochron approach (e.g., DePaolo and Johnson, 1979) can provide a powerful internal reliability criterion. Additionally, internal isochrons can provide information about resetting at the intra-CAI scale and may prove to be especially useful in chronological studies where the astrophysical event is debated.

Al–Mg isotopic studies coupled with detailed petrography show a range of degree of disturbance of the Al–Mg system. Large disturbances associated with obvious textural evidence for secondary mineralization are often ascribed to recrystallization and parent body processing (e.g., Fagan et al., 2007). Disturbance of Al–Mg isochrons of CAIs prior to chondrite accretion is also possible and could have important implications for the duration of the solar nebula phase of solar system evolution (MacPherson and Davis, 1993; Podosek et al., 1991; Young et al., 2005). However, nebular disturbances of the Al–Mg system may be difficult to distinguish from those originating on the parent body (cf. Fagan et al., 2007; MacPherson and Davis, 1993). In the nebula, early resetting can be identified through the existence of a well-defined isochron with an elevated intercept. Both the behavior of the isochron and its elevated intercept implies resetting while ^{26}Al was still present (Young et al., 2005). Notably, an elevated $^{26}Mg^*$ intercept would only occur in a system that has had significant Mg exchange between low Al/Mg and high Al/Mg phases (e.g., Podosek et al., 1991). The greater modal abundance of the high Al/Mg phase (e.g., anorthite), the more leverage it could have had on the system and therefore on the $^{26}Mg^*$ intercept (cf. Young et al., 2005).

Here we focus on one particular type of nebular resetting, that occurring in an open system where exchange occurs between CAIs and the ambient gas surrounding them. We believe that open system resetting was an important process in the formation of nebular solids in general and in CAI Al–Mg isotope systematics in particular. This paper primarily considers large coarse-grained CAIs typical of CV chondrites, nearly all of which have experienced various forms of reprocessing.

The effects of solid-state isotopic exchange (Mg self diffusion) with an infinite gas/chondrite matrix reservoir due to thermal heating and production of $^{26}Mg^*$ from ^{26}Al decay are described in Fig. 1 where they are contrasted with closed-system resetting. Fig. 1 illustrates that the differences between closed and open-system resetting of Al–Mg isochrons are most easily identified when both *in situ* and bulk measurements are made on the same object. The distinguishing features of these systems include an upward shift of the $\delta^{26}Mg^*$ isochron intercept relative to solar system initial in the closed system case and a downward shift in the bulk $\delta^{26}Mg^*$ composition relative to melilite in the open system case. These effects are quantified in what follows and provide constraints on the initial $(^{26}Al/^{27}Al)_0$, temperature, and time that could lead to the range of Al–Mg systematics observed.

In the closed system case the weighted average for a bulk CAI follows the simple "lever rule". At any given time, ^{26}Mg atoms must be conserved in the system and therefore the loss of $^{26}Mg^*$ in high Al/Mg phases results in a corresponding gain of $^{26}Mg^*$ in low Al/Mg phases, as described previously by Podosek et al. (1991). This rocking will lead to a raise in the $^{26}Mg^*$ intercept (left panel in Fig. 1). In the open system example where the surrounding reservoir has abundant Mg relative to Al (and therefore abundant non-radiogenic Mg relative to $^{26}Mg^*$) there will be no rise in the $\delta^{26}Mg^*$ intercept. In this case, the

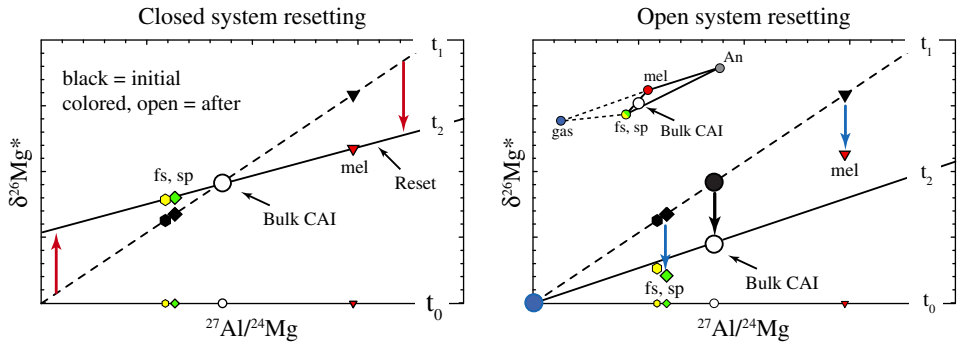

Fig. 1. Schematic Al–Mg isochron diagrams showing examples of: (left) closed system and (right) open system resetting. In the close system case the weighted average for a bulk CAI follows the "lever rule" and will lead to a rise in the $^{26}Mg^*$ intercept (left). In the open system example where the surrounding reservoir has abundant normal Mg, there will be a downward shift in the bulk $\delta^{26}Mg^*$ composition relative to melilite (right) and no rise of the $\delta^{26}Mg^*$ intercept. In this case, the weighted average of the bulk CAI is a function of multi-component mixing as shown graphically. The decrease in $\delta^{26}Mg$ of the bulk reflects a mixture of the minerals that each exchange Mg differentially with gas according to their respective effective diffusion size and rate (explained in detail in the text).

weighted average of the bulk CAI is a "multi-component" mixture (an isotopic mixture along the y-axis between gas and the CAI minerals and an elemental mixture among the minerals—see inset). The relative decreases in $\delta^{26}Mg$ for each component depend on their effective diffusion size and rate (shown graphically in the right panel of Fig. 1 and explained in detail next). These end-member cases can be complicated further because it is also possible to have only partial resetting prior to complete ^{26}Al decay (discussed in detail below).

In the closed system case (Fig. 2, left) the amount of $^{26}Mg^*$ measured (t_∞) equals the total amount originally produced. At time (t_2), if complete resetting occurs, $^{26}Mg^*$ is homogenized among the individual minerals and therefore each has the same values as the

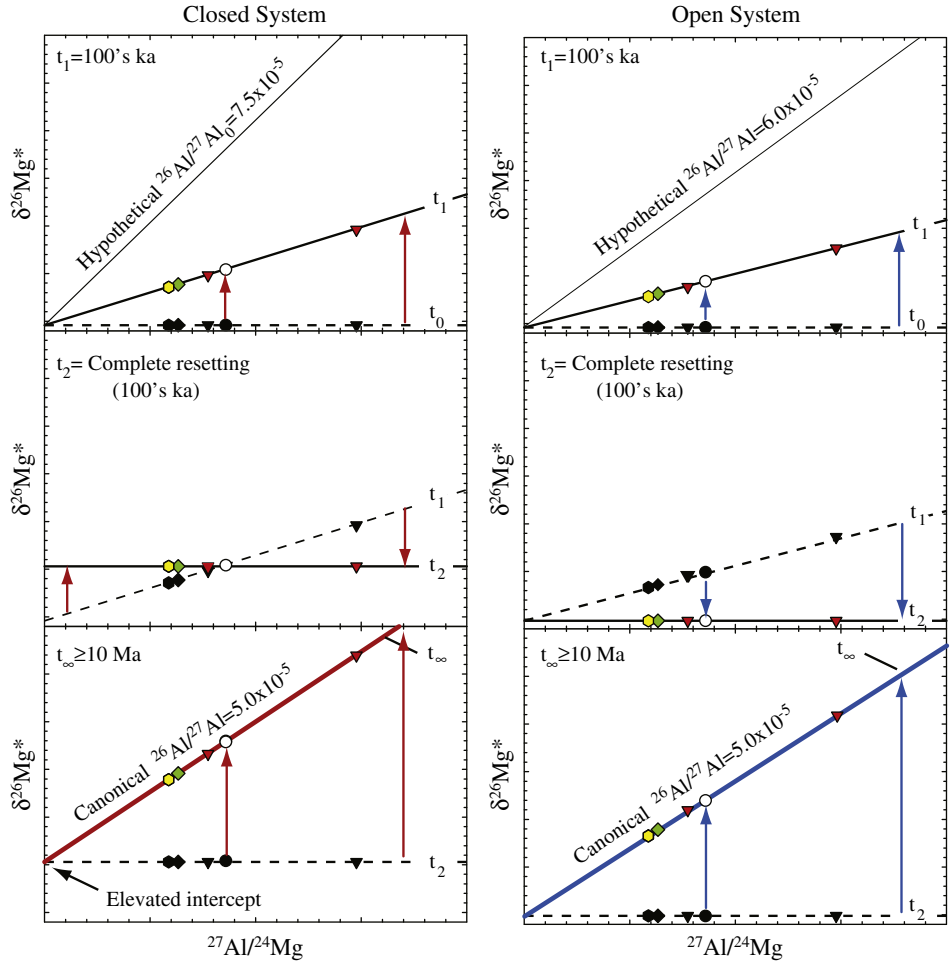

Fig. 2. Schematic time series of the Al–Mg isochron system during complete resetting for: (left) closed system and (right) open system CAI histories. A limited range of hypothetical supra-canonical $^{26}Al/^{27}Al$ values (~$6–7.0\times10^{-5}$) could be reset prior to complete ^{26}Al decay leading to apparent canonical $^{26}Al/^{27}Al$ values (both in bulk and for mineral data). Colored mineral symbols show compositions after decay and/or resetting has completed in each step and in the final step ($t_\infty \geq 10$ Ma) as would be measured. A canonical Al–Mg isochron with an elevated intercept is characteristic of closed system resetting whereas one with a fixed origin (i.e., chondritic initial) is consistent with open system resetting.

bulk. Prior to resetting and after it (if ^{26}Al has not decayed completely) the ^{26}Mg* of each mineral phase will increase directly proportional to its Al/Mg ratio. The increase in the ^{26}Mg* intercept value (and bulk object) when compared to chondrite values is the best evidence that closed system resetting occurred early prior to complete ^{26}Al decay. In the open system case (Fig. 2, right) the intercept ^{26}Mg* value may never increase (i.e., because it was continuously diluted by normal Mg) or perhaps by a small fraction of that produced by closed-system resetting. If *complete* resetting occurs by an open system process, the ^{26}Mg* of individual minerals will each match the chondritic initial value. In this case, resetting of a supra-canonical initial ^{26}Al/^{27}Al value is rendered indistinguishable from a canonical initial ^{26}Al/^{27}Al.

Partial resetting by closed or open system processes can lead to a range of behavior for minerals on Al–Mg isochron diagrams. If some CAIs were only partially reset, and if supra-canonical initial ^{26}Al/^{27}Al existed, then these partially reset CAIs may retain residual supra-canonical signatures that can be recognized (e.g., 144A see Section 4). This is because Mg self diffusion is faster in some minerals than in others. Because of the differences in the rates of diffusion and the differences in crystal dimensions, some phases will tend to approach equilibrium more quickly than others (e.g., spinel with a high Mg self diffusion coefficient and a small dimension). This can be seen graphically in Fig. 3 where the high Al/Mg minerals partially exchange ^{26}Mg* with low Al/Mg minerals, "rocking" each towards a horizontal line trending through an intermediate bulk composition. Because small phases are usually enclosed within larger phases, in addition to their diffusive behavior, their ability to equilibrate with an external reservoir may depend, in part, on diffusion in the host phase and on diffusion along grain boundaries. With all else held constant any rise in the ^{26}Mg* intercept during partial resetting will be less than or equal to that of the completely reset cases. In the open system case all minerals (and therefore the bulk value) will shift down towards the composition of the ambient environment at the time of resetting (e.g., chondritic Mg isotope ratios).

The dynamical nature of the early solar system (e.g., Ciesla, 2007) and the high degree of radial transport within the protoplanetary disk (i.e., Brownlee et al., 2006), give a good reason to believe that resetting of the Al–Mg system in CAIs may reflect both: (1) closed system isotope homogenization of ^{26}Mg* produced *in situ* by radioactive decay of high Al/Mg phases and (2) open system isotope exchange (i.e., "dilution") with a surrounding gas with significant partial pressures of Mg (P_{Mg}). Interpretation of Al–Mg data are further complicated in CAIs where secondary events preferentially alter mineral chemistries, which undoubtedly happened for inclusions that have mineral data that plot below the canonical line, e.g., Podosek et al. (1991). Resetting and partial re-equilibration can also lead to mineral data that plot above the canonical line (Fig. 4.). In the hypothetical case, as previously described by Podosek et al. (1991),

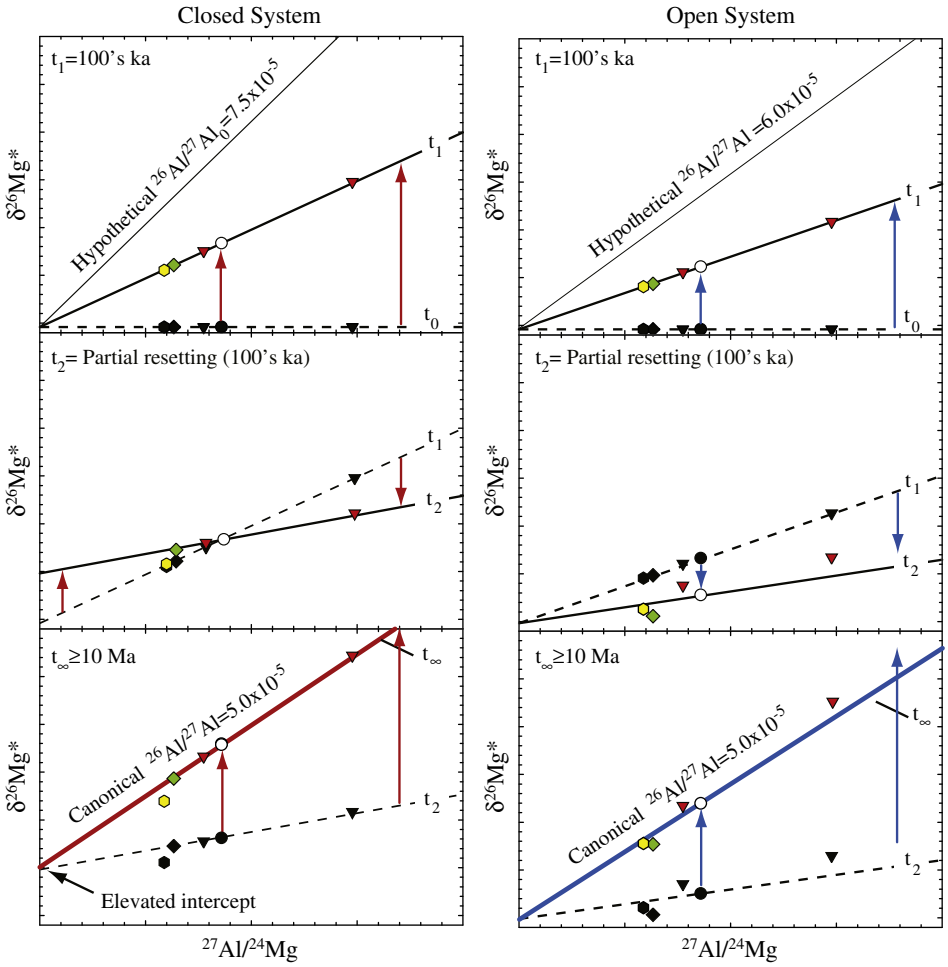

Fig. 3. Schematic time series of the Al–Mg isochron system during partial resetting for: (left) closed system and (right) open system CAI histories. A limited range of hypothetically supra-canonical ^{26}Al/^{27}Al values (~6–7.0×10^{-5}) could be partially reset prior to complete ^{26}Al decay such that subsequent ingrowth of bulk CAIs yield values indistinguishable from canonical ^{26}Al/^{27}Al values, but where some residual materials maintain a vestige of their supra-canonical initial values. Colored symbols indicate mineral compositions after decay and/or partial resetting have occurred for each step and in the final step ($t_\infty \geq 10$ Ma) as would be measured. A canonical Al–Mg isochron with an elevated intercept is characteristic of closed system resetting whereas one with a fixed origin (i.e., chondritic initial) is consistent with open system resetting. Early partial resetting would lead to predictable dispersion among mineral phases for both cases (see figure and text).

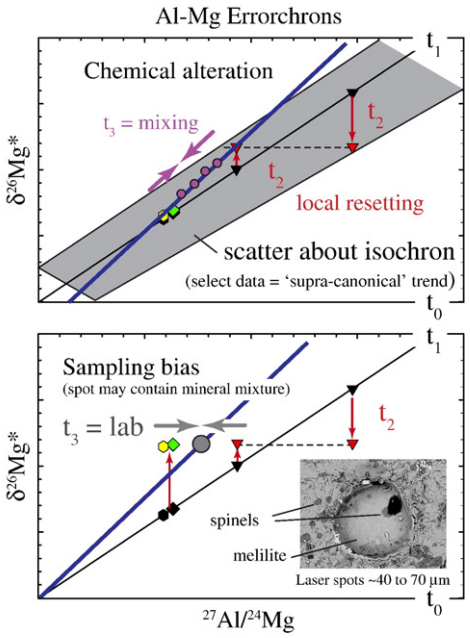

Fig. 4. Schematic Al–Mg plots showing potential errorchrons produced by: (upper) late stage alteration (e.g., of the sort described by Podosek et al. 1991) and (lower) sampling bias because laser spot analyses contain multiple minerals that lead to apparent shifts in the Al/Mg value (see text). If one erroneously calculates a slope between the relict low Al/Mg phases and partially re-equilibrated melilite the result produces a spurious 'supra-canonical' line (upper panel). Likewise, data that reflect spurious analytical mixtures might also be mistaken for evidence of a 'supra-canonical' slope (lower panel). Inset: backscattered scanning electron image shows that typical melilite laser spot analysis (i.e., Young et al., 2005) includes minimal spinel. Because Mg exchange may occur more readily in spinel, the analysis of melilite that contains spinel with excess $\delta^{26}Mg^*$ could appear 'supra-canonical'. Both errorchron types require localized inter-mineral isotopic exchange and inherited radiogenic ^{26}Mg from higher Al/Mg phases. This type of exchange would produce scatter about the initial isochron, but there is no reason that a population of such data would produce a "wedge" (e.g., Fig. 8).

some of the original phases will remain along the original isochron and new (reset) phases will plot along a horizontal line with an elevated $\delta^{26}Mg^*$ value. Upon partial re-equilibration melilite and anorthite react and the result will be that some or all of the melilite migrates upward isotopically. In this case, if one erroneously calculates a slope between the relict low Al/Mg phases (Fig. 4, upper panel) and the newly-formed melilite the result produces a spurious 'supra-canonical' line (Podosek et al., 1991). In contrast, if one calculates a slope between the melilite and the high Al/Mg phases the result would produce a slope consistent with the canonical or lower $(^{26}Al/^{27}Al)_0$ value, but with an elevated intercept (e.g., Young et al., 2005). Furthermore, if partial resetting leads to some phases having elevated $\delta^{26}Mg^*$ values then an artificial mixture between adjacent phases (i.e., during *in situ* analysis in the laboratory) could lead to mineral data plotting above the canonical line. Regression of these inaccurate data might also be mistaken for evidence of a 'supra-canonical' slope (Fig. 4, lower panel).

3. Methods

3.1. Models for resetting

Mass balance calculations are used to show that resetting by an open system process in the protoplanetary disk can explain why most "bulk" CAI analyses exhibit canonical values despite *in-situ* analysis evidence for significant residual intra-CAI supra-canonical material (Fig. 5). Hypothetical minerals used in the illustrative calculations include anorthite ($^{27}Al/^{24}Mg$ ~100 to 300), åkermanitic melilite ($^{27}Al/^{24}Mg$ ~1 to 3.8), gehlenitic melilite ($^{27}Al/^{24}Mg$ ~3.8 to 18.5), spinel ($^{27}Al/^{24}Mg = 2.5$), and fassaite ($^{27}Al/^{24}Mg$ ~2.0 to 3.0). The $^{27}Al/^{24}Mg$

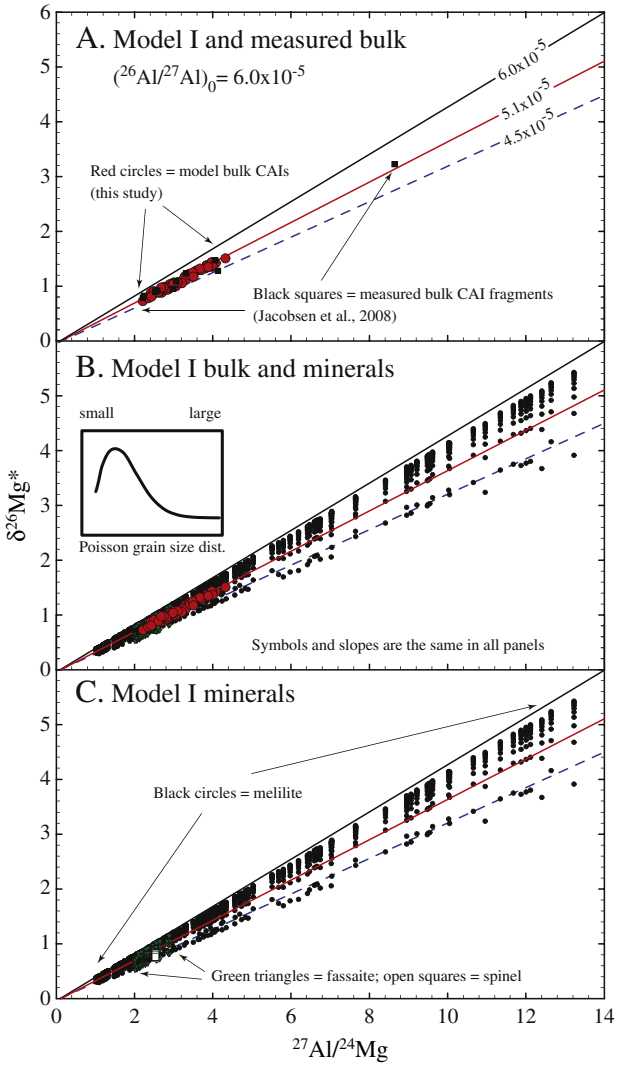

Fig. 5. Representative model results for the Al–Mg system and open system resetting of CAIs. Simulations show resetting behavior of bulk and *in situ* mineral data. In all models $^{26}Al/^{27}Al$ was 5.12×10^{-5} (equivalent to slope defined by measured CAIs, Jacobsen et al., 2008) when resetting occurred. Model I results shown are for a supra-canonical initial value of 6×10^{-5} and a Poisson distribution of crystal sizes (see text). (A) Model bulk CAIs define a canonical errorchron equivalent to measured bulk CAIs. (B) Comparison of model results illustrate that well-behaved canonical bulk CAIs may exhibit a spread (i.e., "wedge") among their individual mineral constituents. Notably a significant fraction of the *in situ* melilite data yields supra-canonical values. (C) Model *in situ* mineral data show a range of values that depend on their effective diffusion sizes and rates. Symbols and $^{26}Al/^{27}Al$ curves are common and defined for all plots.

compositions assigned for minerals that exhibit solid solution were determined at random using a Monte Carlo approach. Given reasonable mineral assemblages, an analogous Monte Carlo approach was used to simulate the modal proportions of phases in each bulk. Eq. (1) comprises the model for each simulated CAI:

$$ {}^{x}R_{\text{bulk CAI}} = \sum_i \left[\left(\frac{C_{Mg,i}M_i}{\sum_i C_{Mg,i}M_i} \right) \left({}^{x}R_{Mg,i}(1-F_i) + {}^{x}R_{Mg,ext}F_i \right) \right] \quad (1) $$

where ${}^{x}R_{\text{bulk CAI}}$ is the isotope ratio of interest for the bulk object, $C_{Mg,i}$ is the number of atoms of Mg per atoms of O in phase i, M_i is the O fraction of phase i (defining the modal abundance of i), ${}^{x}R_{Mg,i}$ is the pre-exchange Mg isotope ratio of phase i, ${}^{x}R_{Mg,ext}$ is the Mg isotope ratio of the external reservoir, and F_i is the fraction of Mg exchanged

for each mineral, respectively. Time dependent excess ^{26}Mg (i.e., ^{26}Mg*) that affects the $^{x}R_{Mg}$ value for each mineral phase i comes from radioactive decay of ^{26}Al obtained using the standard decay Eq. (2):

$$^{26}R_{Mg,i} = \left(\frac{^{26}Mg}{^{24}Mg}\right)_i = \left(\frac{^{27}Al}{^{24}Mg}\right)_i \left(\frac{^{26}Al}{^{27}Al}\right)_t \quad (2a)$$

and

$$\left(\frac{^{26}Al}{^{27}Al}\right)_t = \left(\frac{^{26}Al}{^{27}Al}\right)_0 \exp^{(-\lambda t)} \quad (2b)$$

where $\lambda = 9.52\times10^{-7}$ a^{-1} and t is time. Simulations of isotope exchange occurring in the early solar system in which simulated model times are less than the time required for all ^{26}Al to have decayed to ^{26}Mg* are continued until all of the parent ^{26}Al nuclide is extinct. Isotopic exchange (F_i) used in Eq. (1) based on diffusional transport of Mg entering or leaving a sphere comes from Crank (1975)

$$F_i = 1 - \frac{6}{\pi^2}\sum_{n=1}^{\infty}\frac{1}{n^2}\exp\left(-\Gamma_i n^2\pi^2\right) \quad (3)$$

where $\Gamma = D_i t/a_i^2$ is a dimensionless parameter that is a function of the diffusivity of Mg in each mineral phase D_i, the initial radius of each mineral a_i, and time t. Self diffusion coefficients for Mg for anorthite, melilite, spinel, and fassaite come from Freer (1981); LaTourrette and Wasserburg (1998); Sheng et al. (1991), and reference therein.

Oxygen isotopes, like Mg, in many igneous CAIs show mineral-dependent variations that are plausibly due to gas-CAI exchange (e.g., Ryerson and McKeegan, 1994). This supports the idea that gas-CAI exchanges occurred and might have resulted in mineral-dependent and texture-dependent variations in Mg isotopes. We point out that Mg self diffusion is significantly faster than O self diffusion (Ryerson and McKeegan, 1994) in spinel and will therefore be more easily exchanged (see Fig. 6), explaining why spinel may often retain a more primitive O isotope signal (i.e., Δ^{17}O near 20) while being susceptible to Mg isotopic exchange. Spinel is often found as inclusions within other minerals (see Fig. 4) and thus diffusional shielding may reduce the degree of isotopic exchange between spinel and gas. Nevertheless, with all else constant (e.g., relative location to edge of object, diffusional shielding from surrounding nearest neighbors, etc.) spinel should experience the greatest degree of Mg isotopic exchange based on both its higher Mg diffusivity and its smaller size.

Individual CAIs exhibit a range of grain sizes for many minerals. Additionally, minerals are known to exhibit a range of intra-grain diffusion domain sizes (Lovera et al., 1989). The distinction between a range of independent grain sizes or independent diffusion domain sizes is irrelevant for the purpose of calculating the total fraction (F) of Mg exchanged for each modeled CAI. Several effective grain-size or domain-size distributions were used in the simulations. Although realistic diffusion domain-sizes are not known, we used dimensions that generally match the grain sizes found in typical igneous CAIs (i.e., spinel that was approximately 2× to an order of magnitude smaller than the median sizes — 0.2 to 0.5 cm — used for other minerals). Model parameters explored included various symmetric (e.g., normal Gaussian and uniform) as well as asymmetric (e.g., Poisson and lopsided-bimodal) size distributions. A Poisson distribution skewed towards smaller size fractions may be most realistic and provides the

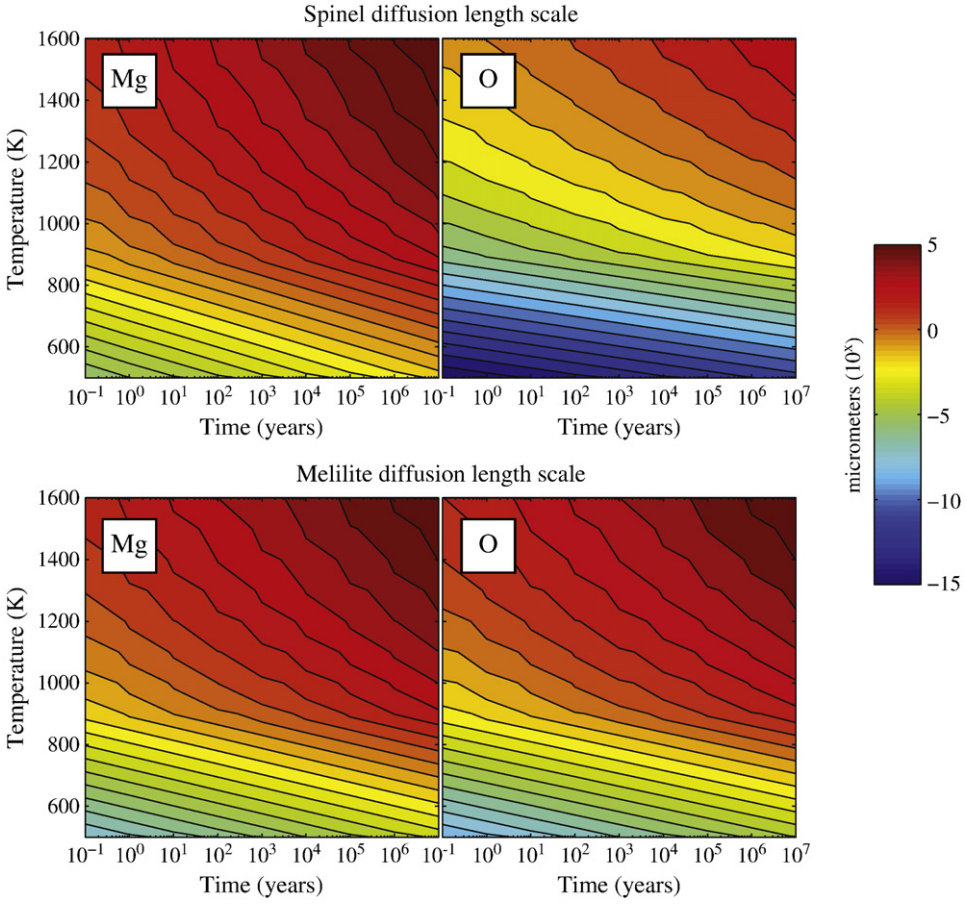

Fig. 6. Temperature dependence of Mg and O diffusion length scales for spinel and melilite (see text). Solid-state diffusion of Mg is similar in melilite and anorthite (LaTourrette and Wasserburg, 1998). Mg exchange by diffusion is faster than O in spinel (Liermann and Ganguly, 2002; Ryerson and McKeegan, 1994). Color scale is equivalent for each plot.

best fit to the observations (Fig. 5). In general conclusions remain unchanged if, for example, a normal Gaussian distribution is used (Fig. 7). The latter models tend to reset more quickly, require longer ingrowth times and/or *lower* supracanonical initial $^{26}Al/^{27}Al$ values to match the measured values because the median size of melilite, anorthite and fassaite grains is more similar in size to spinel. As a check of the veracity of the parameter space used to investigate $^{26}Mg^*$ model results, we use results from a similar model to track the mineral-specific simulated bulk $\delta^{25}Mg$. In detail, this allows us to evaluate the extent of heterogeneity produced within CAIs during mineral-specific isotope exchange (i.e., between the CAIs minerals assumed to be enriched in ^{25}Mg and their surrounding gas of normal Mg isotope composition, i.e., $\delta^{25}Mg = 0$). We deemed as likely those models with $\leq$1.0‰ $\delta^{25}Mg$ isotopic variability due to differential resetting among average mineral compositions (e.g., Model I, see Fig. 5). We consider, end member calculations, i.e., Model II and III as acceptable with $\leq$2.0‰ $\delta^{25}Mg$ isotopic variability (e.g., Fig. 7). This criterion is based on the assumption that the primary mean by which the relatively enriched $\delta^{25}Mg$ values in CAIs are produced is evaporation and not exchange with gas (e.g., Richter et al., 2007; Shahar and Young, 2007).

3.2. Mg isotope composition of CAI minerals by laser ablation MC-ICPMS

Mg isotope measurements reported in this study were included in Young et al. (2005) and collected with a 213 nm ultraviolet (UV) solid-state laser coupled with a multiple-collector double-focusing magnetic-sector inductively coupled plasma mass spectrometer (ThermoFinnigan Neptune™). Analytical methods were described in the appendix of Young et al. (2005), but are briefly described here.

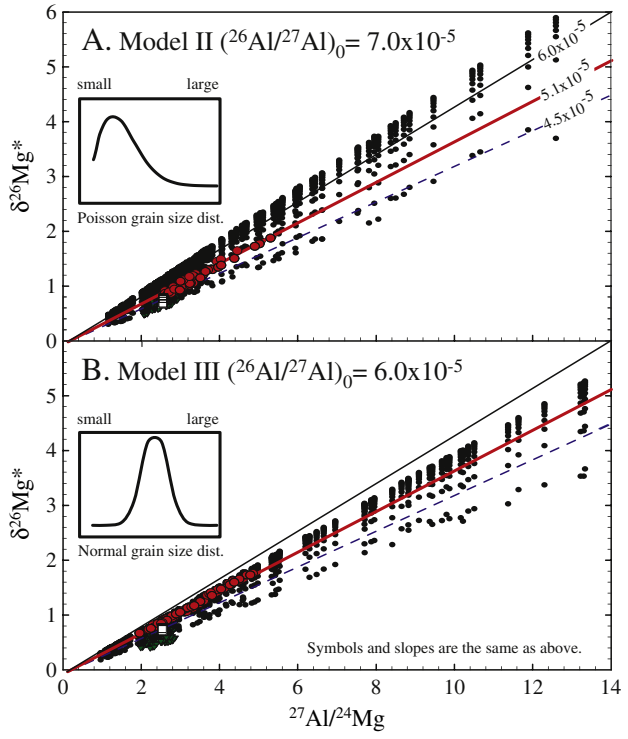

Fig. 7. Acceptable end-member model results for Al–Mg system and open system resetting of CAIs. Several size distributions are considered in simulations (see text): (A) Model II has a Poisson distribution of diffusion domain sizes, $(^{26}Al/^{27}Al)_0 = 7.0\times10^{-5}$, 800 ka of ingrowth prior to resetting, and 50 years of open system Mg isotope exchange at 1600 K . (B) Model III is similar, but has a Gaussian distribution of diffusion domain sizes and $(^{26}Al/^{27}Al)_0 = 6.0\times10^{-5}$. Symbols and $^{26}Al/^{27}Al$ curves in both plots are the same as those in Fig. 5.

In situ analyses were acquired from spots or from line-scans (during which the laser was rastered over a predefined track). Spot size was adjusted from ~40 to 100 μm in order to minimize pit volume while compensating for differences in Mg concentration. Pits are ~20–30 μm deep and are cylindrical. Line-scan widths are ~30–50 μm depending upon the material ablated. The scans are ~10–15 μm deep and ≤300 μm long. Most analyses comprise spots, but scans parallel to CAI edges allow for higher spatial resolution and are useful for analyzing the thin Wark–Lovering rims.

All analyses are reported as linearized per mil deviations from the DSM3 Mg standard (Galy et al., 2003) such that

$$\delta^{X}Mg' = ln\left(\frac{\left(^{X}Mg/^{24}Mg\right)_{unknown}}{\left(^{X}Mg/^{24}Mg\right)_{DSM3}}\right)\times 10^{3} \quad (4)$$

where ^{x}Mg refers to either 25 or 26. We use the logarithm form of the delta notation to linearize the exponential mass fractionation law between $\delta^{26}Mg$ and $\delta^{25}Mg$. Excess radiogenic ^{26}Mg values were calculated from measured $^{26}Mg/^{24}Mg$ and $^{25}Mg/^{24}Mg$ expressed in the linear delta notation (δ') relative to DSM3. Radiogenic ^{26}Mg can be expressed as $\delta^{26}Mg^* \approx \delta^{26}Mg' - \delta^{25}Mg'/(\beta)$ where β is the slope of the mass-dependent isotope fractionation relationship between $\delta^{26}Mg'$ and $\delta^{25}Mg'$. As pointed out by reviewer A. Davis after using δ' values to make the fractionation corrections, δ' values should be converted back to δ values prior to calculating the $\delta^{26}Mg^*$ values. The difference between these two approaches can be a few tenths of a permil in $\delta^{26}Mg^*$ and depends on both $\delta^{25}Mg$ and $\delta^{26}Mg^*$. In the case of Leoville 144A the effect makes the data points a little more supracanonical than they would be with the original equation. Young et al. (2005) corrected their data with $\beta = 0.521$. The reader should be reminded of this lest they take the Young et al.'s (2005) supplemental data table at face value. In this work we used a kinetic value for β of 0.514 recommended by Davis et al. (2005). The general equation for shifts in calculated $\delta^{26}Mg^*$ due to changes in β (e.g., β varying from 0.511 to 0.521) (Young et al., 2002) is $\delta^{26}Mg^*_{corrected} = \delta^{25}Mg(1/\beta_1 - 1/\beta_2)$, a relationship that results in a systematic ambiguity in the accuracy of $\delta^{26}Mg^*$ values in typical CAIs of ~0.2 to 0.3‰ (see discussion by Young and Galy, 2004). The laser ablation approach used here is sufficient to routinely resolve Mg isotope variations of <0.2‰/amu (2σ) and ^{26}Mg excesses of <0.3‰ (2σ).

Values for $(^{26}Al/^{27}Al)_o$ are defined by isochrons comprising linear correlations between $^{26}Mg/^{24}Mg$ and $^{27}Al/^{24}Mg$. Age differences are reflected in the differences in $(^{26}Al/^{27}Al)_o$. Until relatively recently the ability to resolve excess ^{26}Mg by micro-analytical techniques has been largely restricted to the high $^{27}Al/^{24}Mg$ phases (e.g., anorthite with $^{27}Al/^{24}Mg > 100$). Our laser ablation MC-ICPMS measurements were made primarily on the low ($^{27}Al/^{24}Mg$ ~1–16) $^{27}Al/^{24}Mg$ phases (e.g., diopside, spinel, and melilite), but include several anorthite phenocrysts.

4. Model results

4.1. Reset Al–Mg system as recorded by bulk CAIs

Models of Mg isotope exchange between CAIs and their external surroundings reveal that canonical $^{26}Al/^{27}Al$ values could reflect resetting. Table 1 includes a representative summary of reheating histories and corresponding model results. Each simulation starts with a model supra-canonical $^{26}Al/^{27}Al$ initial value, which is reset to the canonical value as a result of reheating and isotope exchange. Supra-canonical initial values of 6 to 7.5×10^{-5} were considered. Based on the prescribed range of initial values, resetting at temperatures of 1500 to 1600 K for ≤100 years at 100's to ~1600 ka after initial CAI formation is found to be required. Later resetting events produced too much inter-mineral stable $\delta^{25}Mg'$ heterogeneity to easily explain the systematic

Table 1
Summary of simulated open system resetting of CAIs.

$(^{26}Al/^{27}Al)_0$	Time elapsed (ka)[a]	Heating (hrs)[b]	$\Delta\delta^{25}Mg$ (‰)[c]	R^2	Model
Early					
7.0×10^{-5}	1600	20	1.2	0.93	
7.0×10^{-5}	800	50	1.6	0.96	II
6.5×10^{-5}	**1200**	**10**	**1.0**	**0.95**	
6.0×10^{-5}	800	50	1.9	0.97	III
6.0×10^{-5}	**800**	**10**	**1.0**	**0.97**	**I**
Late					
7.5×10^{-5}	8000	50	1.5	0.93	
7.0×10^{-5}	8000	10	1.5	0.94	

Bold = best fit and preferred resetting scenarios.
[a] Time between initial condensation and resetting event.
[b] Time at elevated temperature (1500 to 1600 K).
[c] Variance in $\delta^{25}Mg$ between average spinel and melilite.

isotopic zoning profiles of relatively unaltered CAIs. Adherence of a simulated population of CAIs to a well-defined canonical CAI isochron defined by bulk compositions is used to guide the plausibility and therefore the success of the simulations. Fig. 5A shows just such an isochron caused by resetting. The model results match the well-behaved bulk (real fragment) CAI measurements of Jacobsen et al. (2008). In these calculations each simulated bulk CAI is the sum of individual mineral data. The latter can be "sampled" to model *in situ* analyses, as described below (see Section 4.2 and Fig. 5B).

4.2. Reset Al–Mg system of CAIs at mineral to sub-mineral scale

The question is whether early resetting of CAIs leading to canonical $^{26}Al/^{27}Al$ at the bulk (fragment) scale can result in $^{26}Mg^*$ heterogeneity at the scale of individual minerals. Of particular interest is whether the initial abundance of ^{26}Mg excess (i.e., model supra-canonical $^{26}Mg^*$) is resolvable after resetting. A fundamental component of the model calculations reported herein is the conservation of mass. The chemical and isotopic variation among and within each simulated mineral are summed to produce each bulk composition. An account of mass balance at this level would not be possible because data at this level of detail have not been collected from any CAI. The model results reveal that a significant fraction of each bulk CAI, at the mineral to sub-mineral scale, exhibits residual supra-canonical values akin to data reported by Young et al. (2005) and shown for comparison purposes in Fig. 8.

As a consequence of the variable distribution of Mg among constituent phases, whole-rock and internal isochrons are discordant. Mineral specific Mg isotope exchange will lead to a bulk CAI composition in which spinel and anorthite, phases through which Mg isotopes diffuse relatively rapidly, tend to be balanced by the more retentive melilite. Because recent micro-analytical analyses frequently include a significant fraction of melilite, e.g., Young et al. (2005), bulk analysis of the same object (through modeling) or in similar objects (by analytical methods) may yield different results. This is well demonstrated by the structure of the simulated mineral data shown in Figs. 5C and 8 (see inset). A regression of a subset of the model "*in situ*" mineral data for any of the simulated bulk CAIs yields residual information regarding the initial supra-canonical initial $^{26}Al/^{27}Al$ whereas each CAI in bulk falls along the well-defined canonical trend line (see Fig. 5A). In detail, model assumptions related to the size distribution of diffusion length-scales will affect the structure of the simulated *in situ* mineral data. Several grain size distributions and/or diffusion domain size models (e.g., Poisson, Gaussian, and uniform) will produce "the wedge" seen in 144A (Young et al., 2005), see Section 4. Qualitatively, a Poisson distribution seems to provide the best match (Fig. 5).

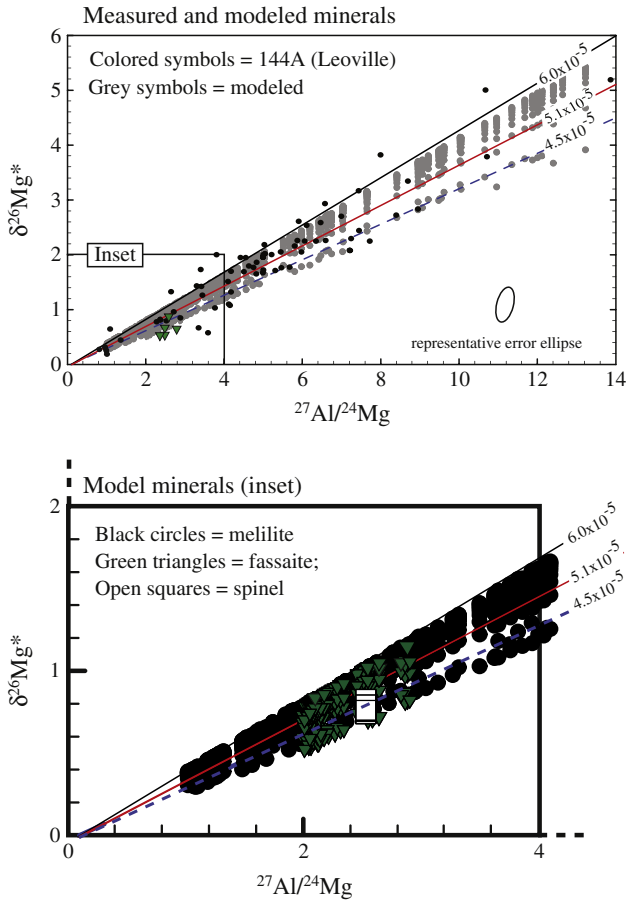

Fig. 8. An Al–Mg isochron diagram showing a direct comparison of representative model mineral results (as in Fig. 5C) to measured *in situ* data of 144A (Leoville, Young et al., 2005). Lower panel is an inset of the upper panel from near the origin showing a detailed behavior of the modeled minerals. The slight $\delta^{26}Mg^*$ deficiency observed in the modeled fassaite (upside down triangles) match that measured in 144A. Symbols and $^{26}Al/^{27}Al$ curves in both plots are the same as those in Fig. 5.

5. Measured Al–Mg system in CAIs

5.1. Representative CAI records

As a "proof of concept", we consider previously obtained data for three well-characterized igneous CAIs from CV3 carbonaceous chondrites. These objects were chosen because they contain mineral phases and textures that are typical of CV3 CAIs. One (Leoville 144A) exhibits significant evidence for supra-canonical $^{26}Al/^{27}Al$ by *in situ* methods. The other two objects (Allende 3576–1 "b" and Efremovka E44) measured by the same *in situ* technique in the same lab at approximately the same time do not. Leoville 144A is a compact, oval-shaped inclusion measuring ~10 mm in length and ~6 mm in width. It is primarily composed of fine-grained melilite ($Åk_{10-25}$) (Young et al., 2000) with an igneous texture, and thus is classified as a compact Type A CAI (Fig. 9). It has a relatively spinel-poor melilite zone that resembles the melilite mantle typical of Type B CAIs. The inner edge of this melilite zone is demarcated by the sudden onset of spinel-rich melilite that is a characteristic of the core. Allende 3576–1 "b" is an irregular inclusion measuring ~4 mm in length and ~3.5 mm in width. Its interior is composed mainly of intergrown melilite and Ti–Al-rich diopside (i.e., fassaite) surrounded by a thin outer melilite mantle (Fig. 10). Efremovka E44 is an oval shaped Type B inclusion measuring ~10 mm in length and ~7 mm in width. It is composed of coarse gained melilite, Ti–Al-rich diopside, and anorthite phenocrysts. Wark–Lovering rims surround each of these objects. Each rim is composed of characteristic (spinel + hibonite → melilite → Ti-rich pyroxene) concentric mineral banding of varying thickness.

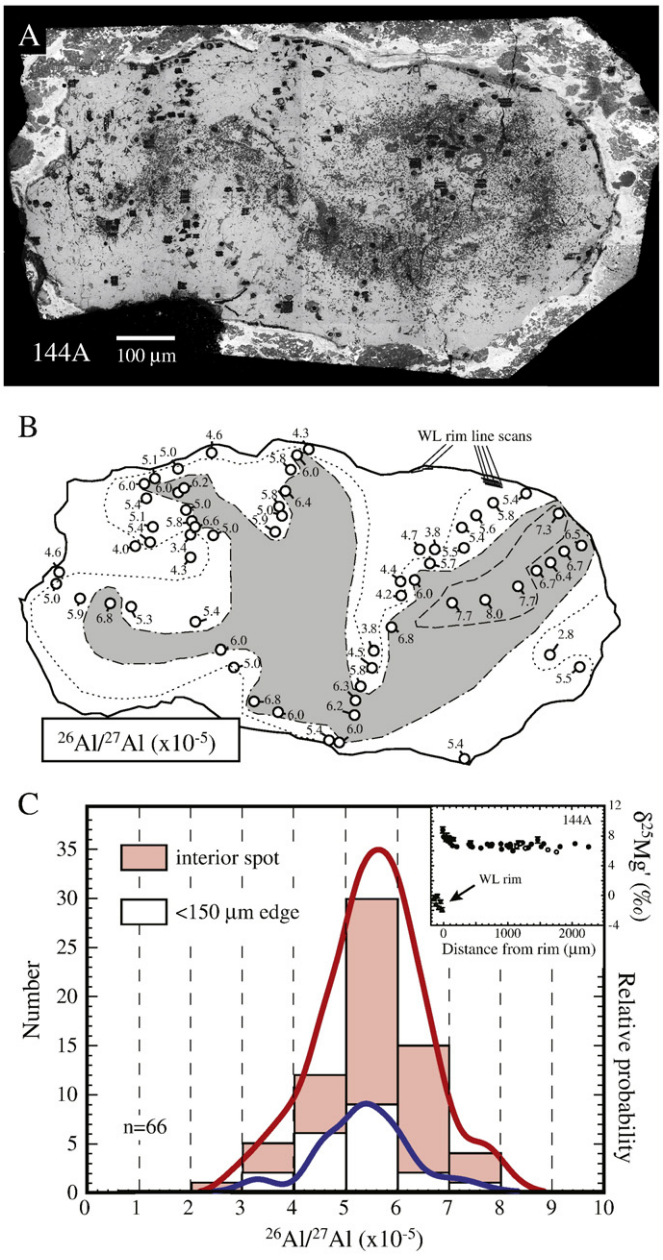

Fig. 9. Backscattered scanning electron image of 144A with companion sketch map and histogram of measured $^{26}Al/^{27}Al$ values. A. Image shows coarse-grained texture of 144A in which melilite is the dominant phase. Darker speckled regions towards interior of CAI are concentrations of spinel grains. Dust from ablation can cause a darkening around the circular analyses pits (Young et al., 2005). Unlabeled square pits are from previous O isotope study (Young et al., 2000). B. Sketch shows model $^{26}Al/^{27}Al$ values ($x10^{-5}$) values for individual spot analyses, see text. Contour lines show zoning in $^{26}Mg^*$, arguably due to minor amounts of isotopic exchange with an external reservoir of normal Mg. Dashed contour line delineates region where $^{26}Al/^{27}Al \geq 7.0$, dash-dot line indicates 6.0, and dotted line indicates 5.0. C. Stacked histograms and probability density functions (PDFs) show slightly supra-canonical mode and spread in model $^{26}Al/^{27}Al$ values. Two-point model $^{26}Al/^{27}Al$ values for individual spot measurements yielding uncertainties better than 1.5×10^{-5} are shown (see text). Red histogram and PDF indicate interior spots and white histogram and blue PDF indicate spots <100 µm from rims. Inset shows stable Mg isotope zoning profile of CAI interior and Wark–Lovering (WL) rim.

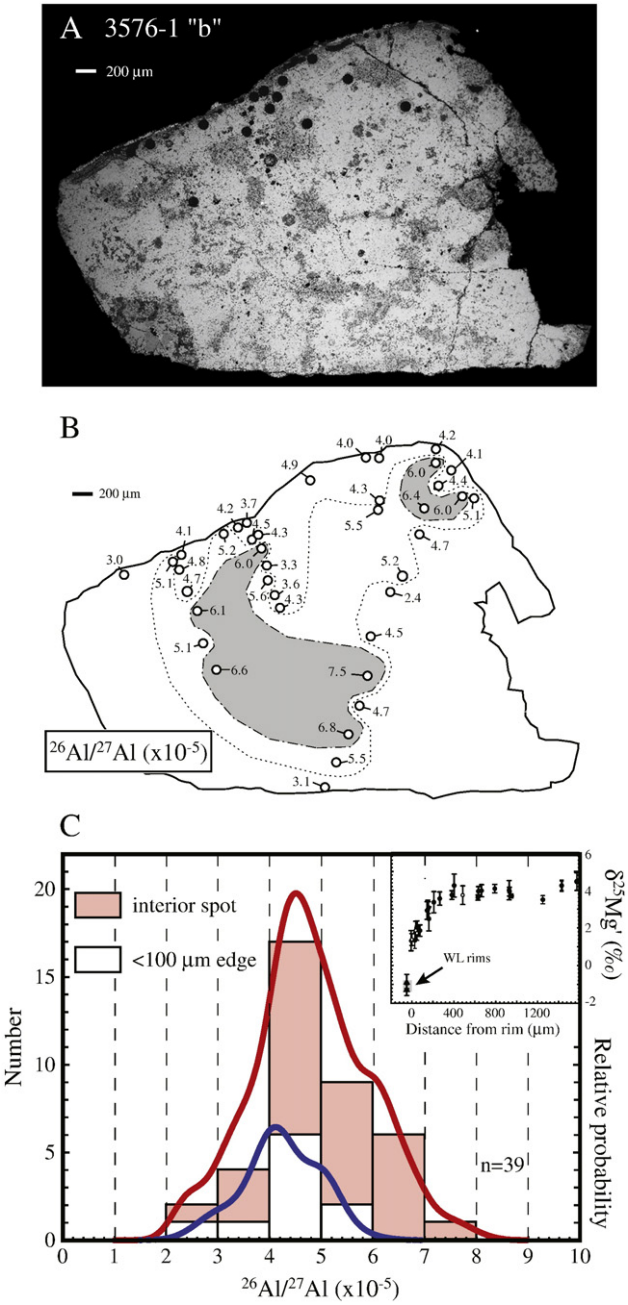

Fig. 10. Backscattered scanning electron image of 3576-1"b" with companion sketch map and measured $^{26}Al/^{27}Al$ values. A. Image shows that CAI is made of melilite = light gray, Ti–Al-rich ("fassaitic") pyroxene = medium gray, and spinel = dark gray. Dust from ablation causes a darkening around the pits. Relatively large circular pits made during Si isotope study (Shahar and Young, 2007), obtained after Mg measurements. B. Sketch shows model $^{26}Al/^{27}Al$ values ($x10^{-5}$) values for individual spot analyses (see text). Heterogeneity in $^{26}Al/^{27}Al$ delineated by contour lines. Dash-dot contour line indicates $^{26}Al/^{27}Al \geq 6.0$ and dotted line indicates 5.0. C. Stacked histograms and probability density functions (PDFs) show canonical mode with slight shoulder and spread in model $^{26}Al/^{27}Al$ values. Two-point model $^{26}Al/^{27}Al$ values for individual spot measurements yielding uncertainties of better than 1.5×10^{-5} are shown (see text). Red histogram and PDF indicate interior spots and white histogram and blue PDF indicate spots <100 µm from rims. Inset shows stable Mg isotope zoning profile of CAI interior and Wark–Lovering (WL) rim.

5.2. Radial $\delta^{25}Mg'$ zoning profiles in CAIs

Spatial variations in $^{25}Mg/^{24}Mg$ within CAIs provide evidence for open-system exchange with their external environments. Many igneous CAIs have positive $\delta^{25}Mg'$ values relative to terrestrial materials. Their high $\delta^{25}Mg'$ values are generally consistent with mass-dependent isotope fractionation during volatilization (cf. Davis et al., 1990). However, edgeward variability in $\delta^{25}Mg$ appears to represent isotopic exchange that postdates volatilization. For example,

there are distinctive edgeward decreases in $\delta^{25}Mg'$ in many CAIs, including 3576–1 "b" and E44 while others like 144A show no such decrease. In the former, $\delta^{25}Mg'$ becomes progressively lower towards the edge over a radial distance of ≤100 μm (inset Fig. 10 and Appendix Figures B and C). The systematic edgeward $\delta^{25}Mg'$ decreases apparently represent a sub-solidus diffusion profile indicating that some CAIs have experienced an open-system exchange with a chondritic Mg reservoir (Simon et al., 2005; Simon et al., 2006). CAI 144A exhibits no evidence for an edgeward $\delta^{25}Mg'$ decrease and in detail, representing multiple traverses across the object, one finds an edgeward increase in $\delta^{25}Mg'$ that is almost a mirror image of the other two CAIs (inset Fig. 9 and Appendix Figure A). The outer ~150 μm margin, composed of mostly melilite, has relatively high $\delta^{25}Mg'$ values up to ~8‰ despite the surrounding Wark–Lovering (WL) rim and matrix (144A spot 64) having subchondritic and chondritic $\delta^{25}Mg'$ values, respectively. Compared to the boundary region, the $\delta^{25}Mg'$ values of the interior of 144A are slightly lower and homogenous (i.e., the interior most portion of the zoning profile is flat across several mm). Some sub-solidus open system exchange is possible because its original zoning profile is unknown, but it was probably less than that in CAIs that exhibit decreasing $\delta^{25}Mg'$ towards their edges.

5.3. Internal Al–Mg isochron correlations with initial $^{26}Al/^{27}Al$ ratios

The ^{26}Al–$^{26}Mg^*$ systematics of the CAIs included here are reminiscent of the effects produced by our open system calculations. As expected, the data do not comprise a single isochron, but rather define a characteristic "wedge" (i.e., there is a spread, but the data tend towards a near zero intercept) composed of what appear to be vestiges of isochrons (compare the agreement between model data and measured data in Fig. 8 and Appendix Figures A–C). The CAI samples describe herein exhibit ^{26}Al–$^{26}Mg^*$ systematics that define both supra-canonical $(^{26}Al/^{27}Al)_o$ (cf. Young et al., 2005) and canonical $(^{26}Al/^{27}Al)_o$ values (MacPherson et al., 1995). The Al–Mg systematics of these samples are summarized in Table 2. The CAI exhibiting evidence for supra-canonical $^{26}Al/^{27}Al$ CAI (144A) has a $\delta^{26}Mg^*$ intercept that is near, but slightly less than zero. The best fit line of 144A data yields an $(^{26}Al/^{27}Al)_0 = 5.82\ (\pm 0.28, 2\ \sigma) \times 10^{-5}$ with an intercept of $\delta^{26}Mg^* = -0.14\ (\pm 0.07, 2\ \sigma)$ ‰, n = 73 or $5.87\ (\pm 0.32, 2\ \sigma) \times 10^{-5}$ with an intercept of $\delta^{26}Mg^* = -0.16\ (\pm 0.08, 2\ \sigma)$ ‰, n = 69 (without the WL rim data) (Appendix Figure A). Best fits to 3576–1 "b" and E44 spot analyses define slopes consistent with the canonical $(^{26}Al/^{27}Al)_0$ value with a near zero to slightly positive $\delta^{26}Mg^*$ intercept. In detail, regression of 3576–1 "b" spot analyses (Appendix Figure B) define a ^{26}Al–$^{26}Mg^*$ internal isochron with a slightly positive intercept of $0.24\ (\pm 0.20, 2\ \sigma)$ ‰, n = 41 or a near zero intercept of $\delta^{26}Mg^* = 0.11\ (\pm 0.24, 2\ \sigma)$ ‰, n = 39 (without WL rim data). E44 data (Appendix Figure C) define a near zero intercept (without anorthite data), but define a clearly positive intercept $\delta^{26}Mg^* = 0.52\ (\pm 0.16, 2\ \sigma)$ ‰, n = 30 (for the melilite and anorthite analyses). As explained above, positive intercepts likely indicate closed system resetting after or during ingrowth of $^{26}Mg^*$ (cf. Young et al., 2005). Subtle differences among the $\delta^{26}Mg^*$ data can be more readily seen in terms of deviations from the canonical line, $\Delta\delta^{26}Mg^*$, versus $^{27}Al/^{24}Mg$. A companion plot for each Al–Mg evolution diagram in the Appendix figures shows these deviations. Portrayed this way, one can see that distinct errochrons defined by different mineral phases may exist within an individual CAI. For example, while the melilite ± anorthite in E44 define a canonical Al–Mg evolution line that has a non-zero intercept of ~0.5‰, the Ti–Al-rich diopside in E44 falls on a canonical Al–Mg evolution line with a fixed zero intercept. Multiple intra-CAI Al–Mg isotopic evolution lines may imply distinct isotopic disturbances and/or retention histories for specific mineral phases (Ito et al., 2004; Podosek et al., 1991; Young et al., 2005, this study).

5.4. Micro-analytical variation of $^{26}Mg^*$ within individual CAIs

In-situ measurement of excess $^{26}Mg^*$ in specific minerals surrounding and/or located at varying distance from their cores demonstrates that some nebular reprocessing and mineral growth occurred after the initial condensation of CAIs. Previously we showed that the Wark–Lovering rims have canonical $^{26}Al/^{27}Al$ values and thus formed in the nebula and not on the parent body (Simon et al., 2005). This result was confirmed by the ion microprobe studies of Cosarinsky et al. (2007), Cosarinsky et al. (2005), and Taylor et al. (2005). Wark–Lovering rim data from 144A, 3576–1 "b", and others define an ^{26}Al–$^{26}Mg^*$ isochron corresponding to an $(^{26}Al/^{27}Al)_0$ value of $5.3\ (\pm 1.6, 2\sigma) \times 10^{-5}$ with a $\delta^{26}Mg^*$ intercept of 0.06 (±0.2, 2σ) ‰. Growth of the Wark–Lovering rims surrounding CAI interiors suggests subsolidus interaction with a relatively high-temperature and high-pressure chondritic gas reservoir (Simon et al., 2005).

Spatial distributions of $^{26}Mg^*$ hint at the presence of diffusion domains within melilites. Regression of spot data from the massive melilite mantle (100's μms) comprising the margin of 144A defines a supra-canonical $^{26}Al/^{27}Al$ value that is consistent with the data from its interior. Likewise, spot analyses within its margin define a population of individual two-point model ^{26}Al–$^{26}Mg^*$ isochrons that is indistinguishable from that calculated for spots from its interior. These model $^{26}Al/^{27}Al$ values are calculated for each spot assuming a fixed origin and typically yield uncertainties less than 1.5×10^{-5} (see stacked histogram in Fig. 9). Each datum was forced through a zero intercept (we recognize that the true intercept is slightly negative, of order −0.03 per mil, based on solar Al/Mg, but this

Table 2
Initial $^{26}Al/^{27}Al$ values for studied CAIs[a].

CAI	N	MSWD	$(^{26}Al/^{27}Al)_0$	$2\sigma_m$ [b]	Intercept	$2\sigma_m$	slope	$2\sigma_m$
Allende 3576–1 "b"	41	1.7	3.83×10^{-5}	0.76	0.24	0.20	0.274	0.05
w/ fixed origin		1.8	4.82×10^{-5}	0.26	*−0.04*	–	0.343	–
No outer edge (<100 μm)[c] and w/fixed origin	30	1.5	5.15×10^{-5}	0.35	*−0.04*	–	0.367	–
Efremovka E44	39	2.1	4.91×10^{-5}	0.32	0.12	0.13	0.346	0.02
w/ fixed origin		2.2	5.23×10^{-5}	0.19	*−0.04*	–	0.372	–
No feldspar	36	2.0	5.29×10^{-5}	0.43	−0.01	0.16	0.377	0.03
Melilite + anorthite only	30	1.0	4.37×10^{-5}	0.35	0.52	0.16	0.307	0.02
Leoville 144A	73	3.4	5.82×10^{-5}	0.28	−0.14	0.07	0.411	0.02
No WL rim	67	3.7	5.87×10^{-5}	0.32	−0.16	0.08	0.412	0.02
w/ fixed origin		3.5	5.49×10^{-5}	0.11	*−0.04*	–	0.388	–

[a] Values are apparent internal isochrons for each CAI.
[b] Uncertainties of $(^{26}Al/^{27}Al)_0$ = listed value $\times 10^{-5}$ ($2\sigma_m$).
[c] The outer 100 μm cutoff is based on the behavior of the $\delta^{25}Mg'$ isotope zoning profile.

distinction is not resolvable with these data). In detail, there is evidence for $^{26}Al/^{27}Al$ zonation in all of the studied CAIs. This can be seen by contouring the two-point model $^{26}Al/^{27}Al$ spot analyses of 3576–1 "b" (Fig. 10) and to a smaller degree those of 144A (Fig. 9). In contrast to 144A, the histogram of $^{26}Al/^{27}Al$ values yielded by 3576–1 "b" is suggestive that its margin has been more reset than its interior (only spots that yield uncertainties of better than 1.5×10^{-5} are shown). Although the zero intercept used to construct the histograms is model dependent, it does not change the fact that spot analyses near the edges (<100 μm from rim) of 3576–1 "b" are skewed towards lower values as compared to the majority of the interior data. When data that are within 100 μm of the rim and the WL rim data are excluded the remaining interior data yield an isochron that defines a $(^{26}Al/^{27}Al)_0$ value of 6.4 (±2.2, 2σ) $\times10^{-5}$ with a $\delta^{26}Mg^*$ intercept of -0.33 (±0.25, 2σ). The melilite mantle in E44 yields a ^{26}Al–$^{26}Mg^*$ isochron with a high $\delta^{26}Mg^*$ intercept and an $(^{26}Al/^{27}Al)_o$ value that is within error, but possibly lower than that characteristic of the CAI as a whole (melilite + diopside). This may reflect isotopic exchange between high and low Al/Mg minerals (cf. Young et al., 2005) and some open system resetting. Evidence for open system behavior is also suggested by the anomalously low $\delta^{25}Mg'$ anorthite data observed within the interior of E44 (see inset of isotope zoning profile in Appendix Figure C).

6. Implications for Al–Mg chronometry of CAIs in the protoplanetary disk

Understanding the origin and extent of isotopic zoning may help explain the apparent discrepancy between the supra-canonical and canonical $(^{26}Al/^{27}Al)_0$ values. We suggest that the observed edgeward decreasing $\delta^{25}Mg'$ zoning profiles reflect sub-solidus modification of the Mg isotopic composition produced initially in CAIs (cf. Simon et al., 2006). Mg isotopic exchange with surrounding chondritic gas during reheating could result in the observed isotopic zoning profiles. Because the original isotopic zoning profile and bulk $\delta^{25}Mg'$ of a given CAI are unknown it is difficult to model its specific formation history. Nevertheless, at face value 3576–1 "b" and E44 have experienced more isotopic exchange than 144A. This is consistent with the isotope exchange models reported herein showing that in bulk the supra-canonical $^{26}Mg^*$ of CAIs has been "diluted" by chondritic Mg. The reheating and partial isotopic exchange may have occurred contemporaneously with internal Al–Mg isotopic resetting (i.e., Young et al., 2005). Collectively these exchange models provide an internally consistent explanation for the existence of rare CAIs with residual evidence for supra-canonical $^{26}Al/^{27}Al$ values and the preponderance of CAIs with canonical $^{26}Al/^{27}Al$ values. Resetting in the nebula is expected to have less effect on the Al/Mg ratios than the Mg isotope ratios of CAIs and their constituent minerals. Mg isotope exchange by self-diffusion rather than chemical diffusion is inferred to be the most important transport mechanism for Mg in CAIs because chemical diffusion of Mg involves charge-balanced coupled substitutions that would also affect the Al (and Si) abundances in the primary mineral phases (i.e., melilite and pyroxene) (Al is stoichiometrically controlled by the Tschermak substitution mechanism). Chemical diffusion of Mg has been shown to be at least two orders of magnitude slower than Mg self-diffusion in melilite (e.g., Nagasawa et al., 2001). This is consistent with the fact that the CAIs studied here have distinctly different $\delta^{25}Mg'$ zoning profiles despite having melilite that exhibit similar and systematic elemental zoning profiles (Fig. 11). Melilite at the margins of the studied CAIs is more gehlenitic (~$Åk_{10}$) than in the interiors. A feature that likely reflects their original igneous crystallization differentiation. In order to directly compare the two profiles in Fig. 11 the relative Al and Mg abundances are reported in terms of the Tschermak exchange vector ($xAl_2Mg_{x-1}Al_{x-1}$), where x is the mole fraction per formula unit of the Tschermak exchange vector. The exchange vector is given by the expression:

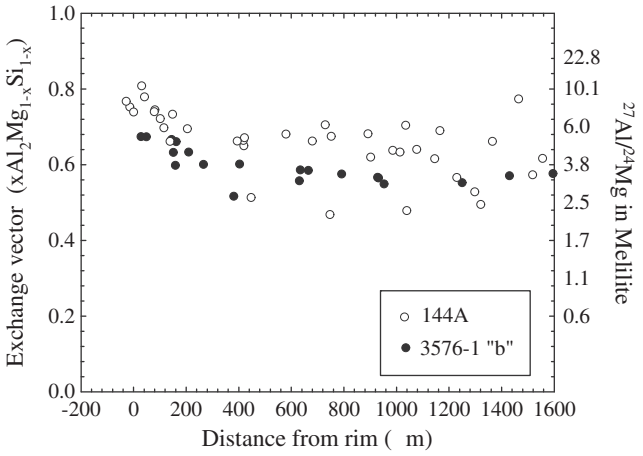

Fig. 11. Comparable Al/Mg zoning profiles in 144A and 34576-b melilite. The composition at exchange vector = 0 is äkermanite and the exchange vector = 1 is gehlenite. The similar compositional trends, despite distinct isotopic zoning profiles, suggests that the chemical profiles are intrinsic to the CAIs and do not reflect later alteration.

$$x = \frac{ab^{24}\mathrm{Mg}\left(^{27}\mathrm{Al}/_{^{24}\mathrm{Mg}_{\mathrm{measured}}}\right)}{\left[2 + ab^{24}\mathrm{Mg}\left(^{27}\mathrm{Al}/_{^{24}\mathrm{Mg}_{\mathrm{measured}}}\right)\right]} \quad (5)$$

where $ab^{24}Mg$ is the abundance of ^{24}Mg and equal to 78.99%. The few anomalously low 144A interior spots likely reflect varying amounts of spinel in the nominally melilite spot analyses.

If the mechanism of thermal reprocessing of CAI interiors needed to lower the $\delta^{25}Mg'$ of the CAI margins is related to conditions and events that also produced the elevated thermal and pressure conditions of Wark–Lovering rim formation (and we believe that they were) then there is a discrepancy between the absolute time difference implied by Al–Mg systematics between Wark–Lovering rims and supra-canonical CAI interiors (of 100's ka) and the model time scales (10^2 to 10^3 years) derived from Eq. (3). This discrepancy is consistent with the idea that canonical $^{26}Al/^{27}Al$ values represent resetting. The decreases in $\delta^{25}Mg'$ towards the edges of the CAIs may reflect one single event 100's to a 1500 ka after initial CAI formation and/or be related to the cumulative time CAIs were immersed in a $>10^{-4}$ bar solar gas and at elevated temperatures. In the later case, the 100's of years time scales would represent an effective time (Σt_i) rather than an absolute time (see below and Fig. 12). Slightly longer nebular reprocessing times would reduce some, but will not eliminate all of the discrepancy between the absolute time and thermal heating time (i.e., time above Mg closure temperature). Numerous short (hours to days) reheating events within the solar nebula is similar to the interpretations of Young et al. (2005) who suggest that the Al–Mg isotope systematics of E44 may have been reset by closed system isotopic exchange due to reheating.

7. Reprocessing CAIs in the protoplanetary disk

The ^{26}Al–^{26}Mg systematics of 144A imply that some CAIs record an interval of Al–Mg isotopic evolution that predates that which is conventionally reported for the solar system (cf. Galy et al., 2004; Taylor et al., 2005; Thrane et al., 2006; Young et al., 2005). Although 144A data define an apparent internal isochron with a well-constrained intercept, excess scatter exists (MSWD = 3.7, n = 73). This scatter (with increasing $^{27}Al/^{24}Mg$ values) could reflect disturbances on the parent

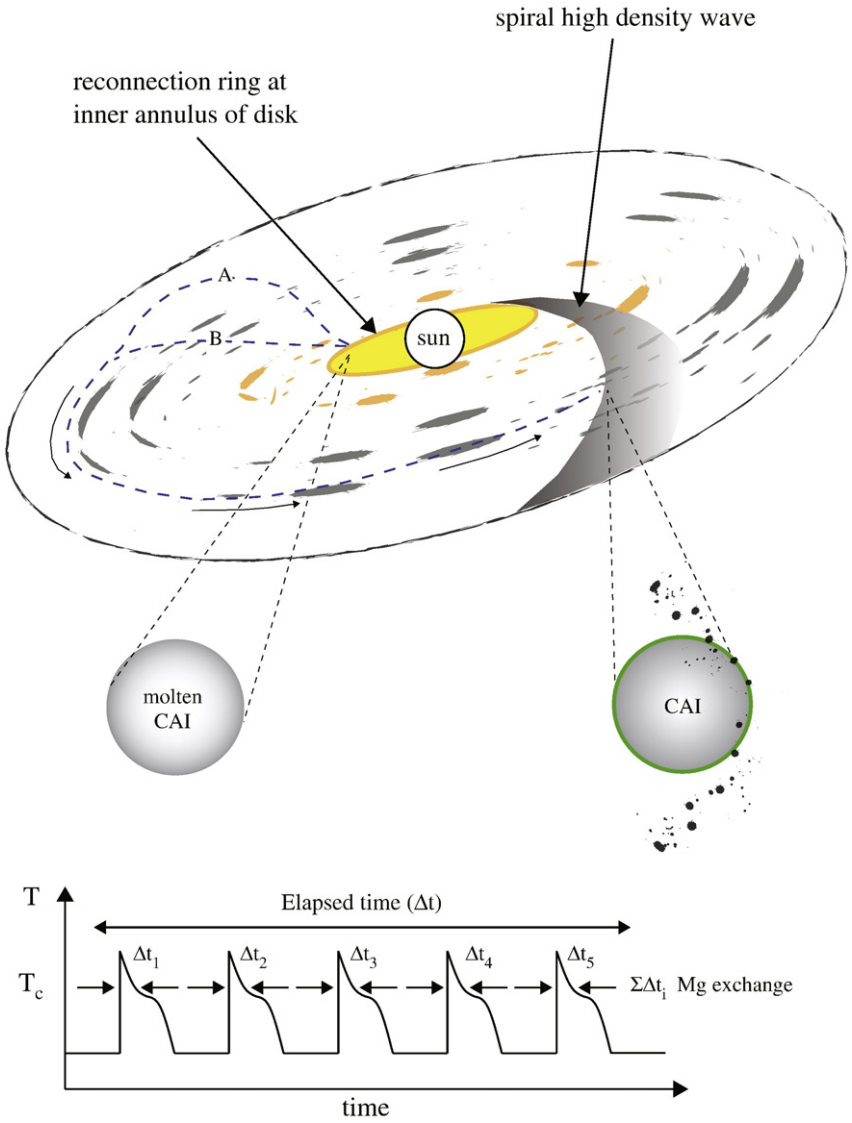

Fig. 12. Environments for thermal possessing of CAIs in the early solar system. Ubiquitous enrichments of heavier Mg in CAIs imply evaporation at high temperatures and low pressures like those predicted near the Sun. Later heating of CAIs could occur as they fall back into the midplane of the disk, indicated by dash path A., as they migrate outward within the plane of the disk, shown as path B, and/or by entering high density waves (i.e., shockwaves). Shockwaves could also be the source for increased dust abundance and Mg partial pressures (see text). The temperature timeline shows a pulsed heating history that would be expected if CAIs passed through shock waves multiple times as they spiral towards the Sun. The total time elapsed (Δt, from ^{26}Al chronology) is distinct from the integrated time (ΣΔt) predicted for CAIs to exist above the closure temperature driving Mg isotope exchange.

body and/or just in the solar nebula. The model calculations (this study) demonstrate that similar scatter (i.e., "the wedge") is an expected result of open system nebular reprocessing. Either way it is clear that only rare CAIs record substantial residual evidence of ^{26}Al abundances greater than the canonical value.

The extant ^{26}Mg* signature of CAIs with supra-canonical $(^{26}Al/^{27}Al)_0$ values and their characteristic Mg isotopic profiles when compared to others with canonical $(^{26}Al/^{27}Al)_0$ values and their distinctive profiles suggest that early in the history of the solar protoplanetary disk (within ~10^5 years of CAI formation) many CAIs were subjected to conditions very different from those where they initially formed. These conditions include P_{Mg} approaching saturation, a gas with near chondritic $\delta^{25}Mg'$, and temperature approaching the solidus for ~10^2 years. The distinctive Mg isotope profiles of the CAIs studied here generally correlate with their characteristic Al–Mg isotope systematics. 144A has a high interior $\delta^{25}Mg'$ and rimward increases in $\delta^{25}Mg'$ values (see Fig. 9 and Appendix Figure A). In contrast, 3576–1 "b" and E44 exhibit lower $\delta^{25}Mg'$ values towards their edges (see Fig. 10 and Appendix Figures B and C). These CAIs also have canonical $(^{26}Al/^{27}Al)_0$ values. E44 exhibits an elevated $\delta^{26}Mg^*$ intercept suggestive of inter-mineral isotope exchange. The depleted $\delta^{25}Mg'$ margins, canonical $(^{26}Al/^{27}Al)_0$, and positive $\delta^{26}Mg^*$ in these CAIs suggest that they experienced Mg isotopic resetting within 10^5 to ~10^6 years of their formation. Elevated intercepts provide important evidence for the degree that isotopic resetting (and therefore reprocessing) occurred prior to complete decay of ^{26}Al. Isotopic disturbances that postdate exhaustion of ^{26}Al decay have been reported for other CAIs (e.g., Caillet et al., 1993; Ito and Messenger, 2007; Kennedy et al., 1997; MacPherson and Davis, 1993) and may also be subtly expressed in these CAIs.

The simple explanation of the data is that solid-state isotopic exchange with a nebular gas and internal Al–Mg isotopic resetting resulted from the *same* reheating mechanism. Moreover it is possible that these events were "marked" by the growth of the Wark–Lovering rims. The differences between $(^{26}Al/^{27}Al)_0$, $\delta^{25}Mg'$ profiles, and $\delta^{26}Mg^*$ intercepts among different inclusions likely reflect their different histories that varied in the degree of resetting and possibly the time period over which the resetting occurred. The record contained

by these CAIs will also depend on their relative proportions of phases with different Al (~radioactive parent nuclei) and Mg abundances. In view of these differences it is likely that CAIs evolved in a nebular environment in which thermal resetting and Mg isotopic exchange occurred periodically.

8. Astrophysical evolution of CAIs

Typical igneous CAIs record a complex nebular history that likely reflects a couple to several astrophysical settings. In the preceding discussions we enumerated how nebular reprocessing occurred in the solid state. The range of distinct physiochemical conditions or "environments" in which CAIs formed is outlined below. Not every CAI need have experienced each environment, nor was each environment necessarily encountered only once. The isotopic record contained within individual CAIs will have been affected by younger events. In many cases all but the most recent event(s) will be lost or obscured. With these caveats, the formation of CAIs examined here likely record the following constraints for evolution of the early solar system.

8.1. Early history of CAIs near the Sun

Initial condensation or migration of protoCAI material into a supersolidus (>1600 K) environment with relatively low Mg partial pressure and low total pressure where melt comprising the CAIs evaporated into space. Incomplete evaporation led to $^{25}Mg/^{24}Mg$ enrichment to varying degrees. This likely occurred by multiple melt evaporation events (Niederer and Papanastassiou, 1984; Simon and Young, 2007) that produced a diffusion-limited molten outer melilite mantle and/or first as a melt in the diffusion regime and then later as a solid leading to the relatively steep, and progressive, edgeward increases in $\delta^{25}Mg'$ (e.g., 144A; Shahar and Young, 2007). All of this happened before canonical time.

8.2. History of CAIs in the proto-planet forming region

A changing nebular environment (ambient and/or by transport of CAIs) to an oxidizing gas with near-saturated P_{Mg} led to the condensation of Wark–Lovering rims (Simon et al., 2005). At nearly the same time reheating partially reset the Al–Mg isotope systematics and promoted Mg isotope exchange between heavier Mg isotope enriched CAI interiors and surrounding nebular Mg-rich gas of chondritic or subchondritic $\delta^{25}Mg'$ composition. This period reflects the integrated time that CAI phases spent above their Mg isotopic closure temperature (Young et al., 2005). This integrated time above the closure temperature was on the order of 10^2 years. We believe that heating in this astrophysical setting produced the preponderance of canonical CAIs. We do not favor the possibility that a very late period of open system isotopic exchange explains CAIs with no $^{26}Mg^*$.

This general two-stage evolution could have occurred within the context of protoplanetary disk evolution if: (1) evaporation occurred while CAIs were near the hot nascent Sun and (2) the CAIs left the low pressure environment and migrated to a midplane environment where they were subjected to episodic heating. A likely candidate for episodic heating is the passage through spiral density waves during migration inward towards the Sun or outward from the Sun by turbulent drag. Fig. 12 shows the hypothetical disk environments where thermal possessing of CAIs may have occurred.

Current theories for the solar nebula, cf. Boss (2004), and references therein, are consistent with these ideas. Evaporative isotopic enrichment of heavier isotopes in protoCAI interiors imply high temperatures and low pressures like those predicted within the inner annulus of disks, e.g., to be later lofted outward by the X-wind, indicated by dash path A (Shu et al. 1996). Later heating of CAIs may have occurred as they fell back into the midplane of the disk or as they migrate outward (Boss and Durisen, 2005; Ciesla, 2007; Cuzzi et al., 2003), shown as path B., and/or associated with encounters with density waves (i.e., shockwaves) (e.g., Hood and Horanyi, 1993; Wood, 1996). Shockwaves could have also been the source for increased dust abundance and Mg partial pressures. Repetitive transport through a shockwave(s) predicts a spiked thermal history that might not be achieved by outward migration alone (Ciesla, 2007). The temperature timeline in Fig. 12 shows a pulsed heating history that would be expected if CAIs passed through shockwaves for multiple times as they were transported near the plane of the protoplanetary disk. A reasonable time scale within the shockwaves is 10^2 years based on the amount of resetting necessary to explain the supra-canonical and canonical values. This time scale is consistent with the total time calculated by Young et al. (2005) required to achieve the internal resetting of the Al–Mg system from supra-canonical to canonical $(^{26}Al/^{27}Al)_0$, as well as, the modeling of Simon et al. (2006) for the formation of the depleted Mg isotopic profiles in the solid-state. This scenario predicts correspondence between the development of CAI margins depleted in $^{25}Mg/^{24}Mg$, *in-situ* evidence of residual supra-canonical $^{26}Al/^{27}Al$ values, the canonical age of Wark–Lovering rims, bulk canonical $^{26}Al/^{27}Al$ CAIs, and evidence for resetting of the Mg isotope system. Studies, such as this that evaluate the detailed chronologic and isotope record contained in CAIs along with their mineralogy can begin to constrain the time scales of important physiochemical processes that modified CAIs. The processes affecting CAIs in turn serve as arbiters for evolution of the solar protoplanetary disk.

9. Future tests of these ideas

The model scenario presented herein can be tested and requires further evaluation. We list next a number of future studies that can be carried out to directly or indirectly help test the ideas in this contribution, they include:

(1) *In situ* stable Mg, Si, and O isotopic studies that carefully document location between analysis spot and grain boundaries for different neighboring minerals in order to show the degree of isotopic heterogeneity among different CAI phases. Such studies are critical for evaluating the degree to which excess ^{26}Mg exchange might have occurred between high Al/Mg and low Al/Mg phases.

(2) *In situ* Al–Mg isotopic studies that systematically document location between the Mg isotope analyses and the edges of CAIs (i.e., zoning profiles) in order to address the correspondence and the prevalence of the characteristic $\delta^{25}Mg$ profiles and Al–Mg chronologies reported herein to test whether dilution by external normal Mg has occurred. Analogous Si and O isotopic zoning profiles across the margins of CAIs could also be used to further examine Mg isotopic evidence for open system isotopic exchange.

(3) Experimental studies that better constrain the anisotropic isotopic diffusivities of relevant CAIs phases (cf. LaTourrette and Wasserburg, 1998), in particular those for melilite.

10. Conclusions

Based on the comparison between simulated resetting of the Al–Mg system in CAIs to representative Al–Mg measurements by LA-MC-ICPMS we suggest a general model for the formation of end-member Mg isotope zoning profiles and $^{26}Al/^{26}Mg$ chronologies. It considers the effect of isotopic exchange with a chondritic gas as a mechanism to explain the range of observed differences. The modeling demonstrates that melilites above the "canonical" errorchron defined by simulated bulk mixtures of the phases (i.e., consistent with the compositions of fragments of CAIs obtained by analysis of acid digested samples)

likely record evidence for residual supra-canonical evolution while the canonical values of the bulk objects themselves are a product of open-system exchange of Mg isotopes. Isotopic exchange could have occurred early (100's ka) and late (~1 Ma) in the solar nebula or much later (>10's Ma) on chondrite parent bodies. The stable Mg isotope composition and excess $^{26}Mg^*$ of Wark–Lovering rims surrounding CAIs (Cosarinsky et al., 2005; Simon et al., 2005) indicate that open system exchange likely occurred prior to and/or during rim formation. Likewise the rim data indicate that nebular conditions characterized by relative high pressures and temperatures, in which open system isotopic exchange is likely to occur, existed at canonical time. Although the modeling here is consistent with a range of supra-canonical values, corresponding to Al/Mg fractionation during condensation and/or the final supersolidus melting event undergone by individual CAIs, the elapsed time between the initial formation of CAIs and their canonical-aged subsolidus isotopic exchange (<100's ka) indicates that the average initial ^{26}Al abundance in the solar system was ~6 to 7×10^{-5}.

Acknowledgements

Discussions with K. McKeegan, A. Davis, M. Ito, Q. Yin, B. Jacobsen, S. Jacobsen, I. Hutcheon, A. Galy, and O. Lovera are greatly appreciated. As are input and sample material provided by S. Russell. Critical and helpful reviews by A. Davis and T. Fagan improve the clarity of the manuscript. This work was supported by grants from the NASA Cosmochemistry program, the NASA Astrobiology Institute, and the National Science Foundation (USA). J. Simon acknowledges support from NASA Johnson Space Center and wishes to thank D. DePaolo and P. Renne for their support of his postdoctoral research over which time some of the ideas and calculations for this contribution originated.

Appendix A. Supplementary data

Supplementary data to this article can be found online at doi:10.1016/j.epsl.2011.02.023.

References

Aléon, J., El Goresy, A., Zinner, E., 2007. Oxygen isotope heterogeneities in the earliest protosolar gas recorded in a meteoritic calcium–aluminum-rich inclusion. Earth and Planetary Science Letters 263 (1–2), 114–127.

Amelin, Y., Krot, A.N., Hutcheon, I.D., Ulyanov, A.A., 2002. Lead isotopic ages of chondrules and calcium–aluminum-rich inclusions. Science 297 (5587), 1678–1683.

Boss, A.P., 2004. Evolution of the solar nebula. VI. Mixing and transport of isotopic heterogeneity. Astrophysical Journal 616 (2), 1265–1277.

Boss, A.P., Durisen, R.H., 2005. Chondrule-forming shock fronts in the solar nebula: a possible unified scenario for planet and chondrite formation. Astrophysical Journal 621 (2), L137–L140.

Bouvier, A., Wadhwa, M., 2010. The age of the solar system redefined by the oldest Pb–Pb age of a meteoritic inclusion. Nature GeoScience 3, 637–641.

Bouvier, A., Blichert-Toft, J., Moynier, F., Vervoort, J.D., Albarede, F., 2007. Pb–Pb dating constraints on the accretion and cooling history of chondrites. Geochimica et Cosmochimica Acta 71 (6), 1583–1604.

Brownlee, D., et al., 2006. Research article — comet 81P/Wild 2 under a microscope. Science 314 (5806), 1711–1716.

Caillet, C., MacPherson, G.J., Zinner, E.K., 1993. Petrologic and Al–Mg isotopic clues to the accretion of 2 refractory inclusions onto the Leoville parent body — one was hot, the other wasn't. Geochimica et Cosmochimica Acta 57 (19), 4725–4743.

Ciesla, F.J., 2007. Outward transport of high-temperature materials around the midplane of the solar nebula. Science 318 (5850), 613–615.

Compston, W., Jeffery, P.M., 1959. Anomalous common strontium in granite. Nature 184 (4701), 1792–1793.

Cosarinsky, M., Taylor, D.J., McKeegan, K.D. and Hutcheon, I.D., 2005. Mg isotopic study of Wark–Lovering rims in Type A inclusions from CV chondrites: formation mechanisms and timing, 68th Annual Meteoritical Society Meeting, pp. Abst. #5284.

Cosarinsky, M., Taylor, D.J., Liu, M.-C., McKeegan, K.D. and Krot, A.N., 2007. Distribution of aluminum-26 in refractory inclusions from CV chondrites., Workshop on Chronology of Meteorites, Hawaii, pp. Abst.# 4052.

Crank, J., 1975. The Mathematics of Diffusion. Clarendon Press, Oxford. 159 pp.

Cuzzi, J.N., Davis, S.S., Dobrovolskis, A.R., 2003. Blowing in the wind. II. Creation and redistribution of refractory inclusions in a turbulent protoplanetary nebula. Icarus 166 (2), 385–402.

Davis, A.M., Hashimoto, A., Clayton, R.N., Mayeda, T.K., 1990. Isotope mass fractionation during evaporation of Mg_2SiO_4. Nature 347 (6294), 655–658.

Davis, A.M., et al., 2005. Isotopic mass fractionation laws and the initial solar system $^{26}Al/^{27}Al$ ratio. Lunar and Planetary Science XXXVI Abst. # 2334.

DePaolo, D.J., Johnson, R.W., 1979. Magma genesis in the New Britain island-arc — constraints from Nd and Sr isotopes and trace-element patterns. Contributions to Mineralogy and Petrology 70 (4), 367–379.

Esat, T.M., Spear, R.H., Taylor, S.R., 1986. Isotope anomalies induced in laboratory distillation. Nature 319, 576–578.

Fagan, T.J., Guan, Y., MacPherson, G.J., 2007. Al–Mg isotopic evidence for episodic alteration of Ca–Al-rich inclusions from Allende. Meteoritics & Planetary Science 42 (7–8), 1221–1240.

Freer, R., 1981. Diffusion in silicate minerals and glasses — a data digest and guide to the literature. Contributions to Mineralogy and Petrology 76 (4), 440–454.

Galy, A., Young, E.D., Ash, R.D., O'Nions, R.K., 2000. The formation of chondrules at high gas pressures in the solar nebula. Science 290 (5497), 1751–1753.

Galy, A., et al., 2003. Magnesium isotope heterogeneity of the isotopic standard SRM980 and new reference materials for magnesium–isotope-ratio measurements. Journal of Analytical Atomic Spectrometry 18 (11), 1352–1356.

Galy, A., Hutcheon, I.D., Grossman, L., 2004. $(^{26}Al/^{27}Al)_0$ of the solar nebula inferred from Al–Mg systematics in bulk CAIs from CV3 chondrites. Lunar and Planetary Science XXXV Abst. # 1790.

Grossman, L., et al., 2000. Major element chemical and isotopic compositions of refractory inclusions in C3 chondrites: the separate roles of condensation and evaporation. Geochimica et Cosmochimica Acta 64 (16), 2879–2894.

Grossman, L., Ebel, D.S., Simon, S.B., 2002. Formation of refractory inclusions by evaporation of condensate precursors. Geochimica et Cosmochimica Acta 66 (1), 145–161.

Hood, L.L., Horanyi, M., 1993. The nebular shock wave model for chondrule formation: one-dimensional calculations. Icarus 106, 179–189.

Hsu, W.B., Wasserburg, G.J., Huss, G.R., 2000. High time resolution by use of the Al-26 chronometer in the multistage formation of a CAI. Earth and Planetary Science Letters 182 (1), 15–29.

Hutcheon, I.D., 1982. Ion probe magnesium isotopic measurements of Allende inclusions. ACS Symposium Series 176, 95–128.

Ireland, T.R., Zinner, E.K., Fahey, A.J., Esat, T.M., 1992. Evidence for distillation in the formation of Hal and related hibonite inclusions. Geochimica et Cosmochimica Acta 56 (6), 2503–2520.

Ito, M. and Messenger, S., 2007. Thermal metamorphic history of a CAI constrained by high spatial resolution Mg isotopic measurements, Workshop of Chronology of Meteorites, pp. Abst. # 4040.

Ito, M., Nagasawa, H., Yurimoto, H., 2004. Oxygen isotopic SIMS analysis in Allende CAI: details of the very early thermal history of the solar system. Geochimica et Cosmochimica Acta 68 (13), 2905–2923.

Jacobsen, B., et al., 2008. Al-26-Mg-26 and Pb-207-Pb-206 systematics of Allende CAIs: canonical solar initial Al-26/Al-27 ratio reinstated. Earth and Planetary Science Letters 272 (1–2), 353–364.

Kennedy, A.K., Beckett, J.R., Edwards, D.A., Hutcheon, I.D., 1997. Trace element disequilibria and magnesium isotope heterogeneity in 3655A: evidence for a complex multi-stage evolution of a typical Allende Type B1 CAI. Geochimica et Cosmochimica Acta 61 (7), 1541–1561.

LaTourrette, T., Wasserburg, G.J., 1998. Mg diffusion in anorthite: implications for the formation of early solar system planetesimals. Earth and Planetary Science Letters 158 (3–4), 91–108.

Lee, T., Papanastassiou, D.A., Wasserburg, G.J., 1976. Demonstration of 26 Mg excess in Allende and evidence for 26Al. Geophysical Research Letters 3, 109–112.

Liermann, H.P., Ganguly, J., 2002. Diffusion kinetics of Fe^{2+} and Mg in aluminous spinel: experimental determination and applications. Geochimica et Cosmochimica Acta 66 (16), 2903–2913.

Lovera, O.M., Richter, F.M., Harrison, T.M., 1989. The Ar-40 Ar-39 thermochronometry for slowly cooled samples having a distribution of diffusion domain sizes. Journal of Geophysical Research-Solid Earth and Planets 94 (B12), 17917–17935.

MacPherson, G.J., Davis, A.M., 1993. A petrologic and ion microprobe study of a Vigarano type-B refractory inclusion — evolution by multiple stages of alteration and melting. Geochimica et Cosmochimica Acta 57 (1), 231–243.

MacPherson, G.J., Davis, A.M., Zinner, E.K., 1995. The distribution of Al-26 in the early solar-system — a reappraisal. Meteoritics 30 (4), 365–386.

Nagasawa, H., Suzuki, T., Ito, M., Morioka, M., 2001. Diffusion in single crystal of melilite: interdiffusion of Al + Al vs. Mg + Si. Physics and Chemistry of Minerals 28 (10), 706–710.

Niederer, F.R., Papanastassiou, D.A., 1984. Ca isotopes in refractory inclusions. Geochimica et Cosmochimica Acta 48 (6), 1279–1293.

Podosek, F.A., et al., 1991. Correlated study of initial Sr-87/Sr-86 and Al–Mg isotopic systematics and petrologic properties in a suite of refractory inclusions from the Allende meteorite. Geochimica et Cosmochimica Acta 55 (4), 1083–1110.

Richter, F.M., Davis, A.M., Ebel, D.S., Hashimoto, A., 2002. Elemental and isotopic fractionation of Type B calcium-, aluminum-rich inclusions: experiments, theoretical considerations, and constraints on their thermal evolution. Geochimica et Cosmochimica Acta 66 (3), 521–540.

Richter, F.M., Janney, P.E., Mendybaev, R.A., Davis, A.M., Wadhwa, M., 2007. Elemental and isotopic fractionation of type B CAI-like liquids by evaporation. Geochimica et Cosmochimica Acta 71 (22), 5544–5564.

Ryerson, F.J., McKeegan, K.D., 1994. Determination of oxygen self-diffusion in äkermanite, anorthite, diopside, and spinel — implications for oxygen isotopic

anomalies and the thermal histories of Ca–Al-rich inclusions. Geochimica et Cosmochimica Acta 58 (17), 3713–3734.
Shahar, A., Young, E.D., 2007. Astrophysics of CAI formation as revealed by silicon isotope LA-MC-ICPMS of an igneous CAI. Earth and Planetary Science Letters 257, 497–510.
Sheng, Y.J., Hutcheon, I.D., Wasserburg, G.J., 1991. An experimental-study of Mg self-diffusion in spinel. Meteoritics 26 (4), 394–395.
Shu, F.H., Shang, H., Lee, T., 1996. Toward an astrophysical theory of chondrites. Science 271 (5255), 1545–1552.
Simon, J.I. and Young, E.D., 2007. Evaporation and Mg isotope fractionation: model constraints for CAIs, Lunar and Planetary Science Conference, League City, Texas, pp. Contribution No. 1338, p. 2424–2425.
Simon, J.I., et al., 2005. A short timescale for changing oxygen fugacity in the solar nebula revealed by high-resolution Al-26–Mg-26 dating of CAI rims. Earth and Planetary Science Letters 238 (3–4), 272–283.
Simon, J.I., Russell, S.S., Tonui, E.K. and Young, E.D., 2006. Reconstructing changing conditions in the solar nebula: Model constraints and evidence from magnesium isotopes in CAIs, Lunar and Planetary Science XXXVII. LPI, League City, Texas, pp. abstract no. 2160.
Stolper, E., 1982. Crystallization sequences of Ca–Al-rich inclusions from Allende — an experimental-study. Geochimica et Cosmochimica Acta 46 (11), 2159–2180.
Taylor, D.J., et al., 2005. Survey of initial ^{26}Al in type A and B CAIs: evidence for an extended formation period for refractory inclusions. 68th Annual Meteoritical Society Meeting, p. 5282.
Thrane, K., Bizzarro, M., Baker, J.A., 2006. Extremely brief formation interval for refractory inclusions and uniform distribution of Al-26 in the early solar system. Astrophysical Journal 646 (2), L159–L162.
Tonui, E.K., Connelly, H.C., McCoy, T., Young, E.D., 2008. Mg isotope study of CAIs by UV laser ablation and solution MC-ICPMS: implications for canonical and supra-canonical evolution. Lunar and Planetary Science XXXIX Houston, pp. Abst. #1380.
Wood, J.A., 1996. Processing of chondritic and planetary material in spiral density waves in the nebula. Meteoritics 31, 641–645.
Young, E.D., Galy, A., 2004. The isotope geochemistry and cosmochemistry of magnesium. Geochemistry of Non-Traditional Stable Isotopes 55, 197–230.
Young, E.D., Russell, S.S., Ash, R.D., 2000. Ultraviolet laser ablation measurements of oxygen isotope ratios in a Leoville compact Type A CAI: Lunar and Planetary Science, XXXI, p. 1837. Houston, Texas.
Young, E.D., Galy, A., Nagahara, H., 2002. Kinetic and equilibrium mass-dependent isotope fractionation laws in nature and their geochemical and cosmochemical significance. Geochimica et Cosmochimica Acta 66 (6), 1095–1104.
Young, E.D., et al., 2005. Supra-canonical Al-26/Al-27 and the residence time of CAIs in the solar protoplanetary disk. Science 308 (5719), 223–227.